Molecular Cell

Article

DNA topology regulates PAM-Cas9 interaction and DNA unwinding to enable near-PAMless cleavage by thermophilic Cas9

Graphical abstract

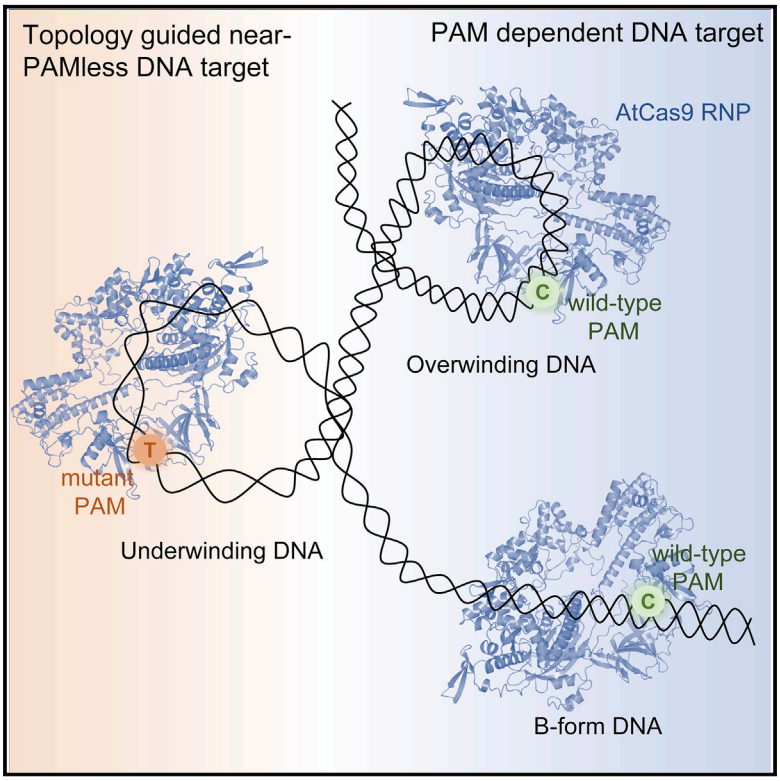

Highlights

- Identification of a thermophilic AtCas9 with broad PAM CNNN and RNNA (R = A/G)
- AtCas9 has a unique PAM-Cas interaction mechanism that can be regulated by DNA topology
- AtCas9 shows near-PAMless cleavage in *E. coli* and effective base editing in 293T cells

Authors

Ya-Jing Shi, Min Duan, Jun-Mei Ding, ..., Xin-Lin Lei, Hao Yin, Ying Zhang

Correspondence

ying.zhang84@whu.edu.cn

In brief

Shi et al. identified a thermophilic AtCas9, which has a relaxed PAM, and the PAM interaction can be robustly regulated by DNA topology. AtCas9 exhibits near-PAMless editing of supercoiled plasmids in *E. coli* and effective base-editing activity in mammalian cells.

Shi et al., 2022, Molecular Cell *82*, 1–16
November 3, 2022
https://doi.org/10.1016/j.molcel.2022.09.032

CellPress

Molecular Cell

CellPress

Article

DNA topology regulates PAM-Cas9 interaction and DNA unwinding to enable near-PAMless cleavage by thermophilic Cas9

Ya-Jing Shi,[1,5] Min Duan,[1,5] Jun-Mei Ding,[2,5] Fan-Qi Wang,[1] Li-Li Bi,[1] Cai-Xiang Zhang,[1] Yi-Zhou Zhang,[1] Jun-Yi Duan,[1] An-Hui Huang,[1] Xin-Lin Lei,[1] Hao Yin,[1,3,4] and Ying Zhang[1,6,*]

[1]Department of Rheumatology and Immunology, Medical Research Institute, Frontier Science Center for Immunology and Metabolism, Zhongnan Hospital of Wuhan University, Wuhan University, Wuhan 430071, China

[2]Engineering Research Center of Sustainable Development and Utilization of Biomass Energy, Yunnan Normal University, Yunnan 650500, China

[3]Department of Urology and Department of Pulmonary and Critical Care Medicine, Zhongnan Hospital of Wuhan University, Wuhan University, Wuhan 430071, China

[4]TaiKang Center for Life and Medical Sciences, TaiKang Medical School, Wuhan University, Wuhan 430071, China

[5]These authors contributed equally

[6]Lead contact

*Correspondence: ying.zhang84@whu.edu.cn

https://doi.org/10.1016/j.molcel.2022.09.032

SUMMARY

CRISPR-Cas9-mediated genome editing depends on PAM recognition to initiate DNA unwinding. PAM mutations can abolish Cas9 binding and prohibit editing. Here, we identified a Cas9 from the thermophile *Alicyclobacillus tengchongensis* for which the PAM interaction can be robustly regulated by DNA topology. AtCas9 has a relaxed PAM of N_4CNNN and N_4RNNA (R = A/G) and is able to bind but not cleave targets with mutated PAMs. When PAM-mutated DNA was in underwound topology, AtCas9 exhibited enhanced binding affinity and high cleavage activity. Mechanistically, AtCas9 has a unique loop motif, which docked into the DNA major groove, and this interaction can be regulated by DNA topology. More importantly, AtCas9 showed near-PAMless editing of supercoiled plasmid in *E. coli*. In mammalian cells, AtCas9 exhibited broad PAM preference to edit plasmid with up to 72% efficiency and effective base editing at four endogenous loci, representing a potentially powerful tool for near-PAMless editing.

INTRODUCTION

Clustered regularly interspaced short palindromic repeats and CRISPR-associated proteins (CRISPR-Cas9) systems, present in 90% of archaea and ~40% of bacteria, serve as the adaptive immune machinery to protect the host from invading nucleic acids (Barrangou et al., 2007; Garneau et al., 2010; Makarova et al., 2011a; Marraffini and Sontheimer, 2008; Wiedenheft et al., 2012). The CRISPR-Cas9 systems contain CRISPR arrays, consisting of identical repeats that are interleaved with unique sequences as "spacer" acquired from foreign invaders, and their adjacent cas genes as their major components (Makarova et al., 2011b). When invaded by foreign DNA, CRISPR arrays are transcribed and processed into CRISPR RNA (crRNA). Cas proteins, guided by crRNA and a *trans*-activating RNA (tracrRNA), act to cleave target DNA that is complementary to the crRNA (Yosef et al., 2012).

To distinguish self versus non-self, CRISPR systems have developed a sequence preference of protospacer adjacent motif (PAM) located in the invader sequence (Marraffini and Sontheimer, 2010). The PAM sequences are different among cas orthologs (Ran et al., 2015; Singh et al., 2016; Sternberg et al., 2015). PAM recognition and binding are essential in initiating local DNA unwinding and the subsequent cleavage (Mekler et al., 2017; Pickar-Oliver and Gersbach, 2019; Sternberg et al., 2014). Current models for DNA unwinding indicate that Cas9 searches and binds to a PAM site, followed by the formation of a directional R-loop extending from the PAM site (Sternberg et al., 2014). The PAM-interacting (PI) domain of Cas9 forms several hydrogen bonds with the PAM bases and the deoxyribose-phosphate backbones, serving as an anchoring point to initiate the unwinding of the target strand (TS) (Jiang and Doudna, 2017; Jiang et al., 2016). After PAM recognition and binding, the ability to fully unwind double-stranded DNA (dsDNA) through base pairing between the spacer of gRNA and the TS is the primary determinant to initiate cleavage activity of Cas9 (Gong et al., 2018). Mutations in PAM block its interaction with the PI domain of Cas9, thereby abolishing DNA unwinding (Datsenko et al., 2012; Singh et al., 2016). DNA unwinding can be regulated by either negative or positive torque in the DNA

Please cite this article in press as: Shi et al., DNA topology regulates PAM-Cas9 interaction and DNA unwinding to enable near-PAMless cleavage by thermophilic Cas9, Molecular Cell (2022), https://doi.org/10.1016/j.molcel.2022.09.032

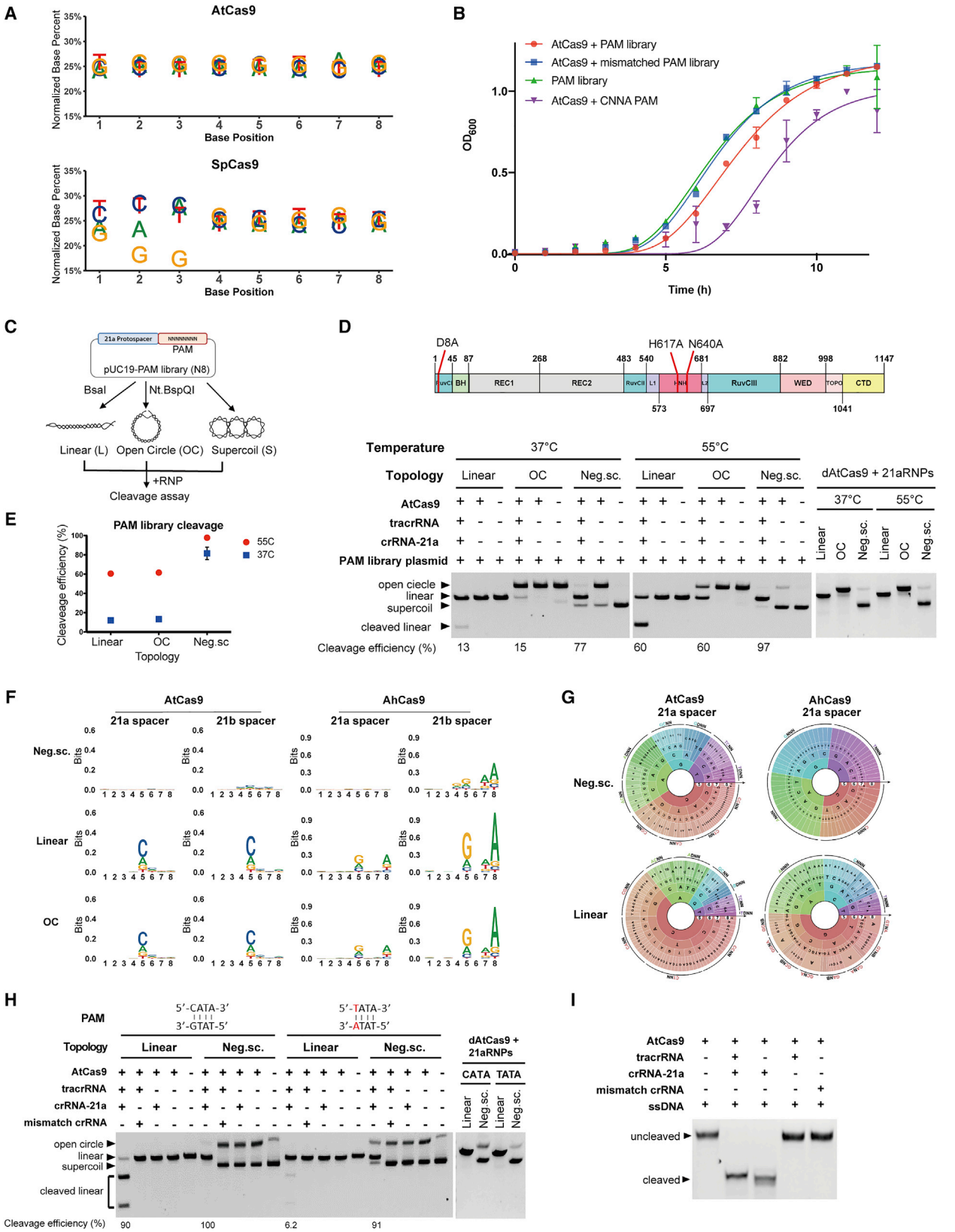

(legend on next page)

(Bustamante et al., 2003; Stolz et al., 2019). Previous studies have indicated that supercoiled DNA can enhance Cas9 cleavage kinetics by facilitating DNA unwinding when PAM is present (Ivanov et al., 2020; Szczelkun et al., 2014). However, whether DNA topology could play a role in regulating PAM recognition and binding remains unknown.

Of the characterized CRISPR-Cas9 systems, type II Cas9 protein—particularly the *Streptococcus pyogenes* Cas9 (SpCas9)—is the most robust and widely used in genome editing. SpCas9, guided by a programmable single-guide RNA (sgRNA) system, effectively cleaves the target DNA at sequences adjacent to an NGG PAM (N = A, T, C, or G) and results in a blunt-ended double-stranded break (Doudna and Charpentier, 2014; Sontheimer and Barrangou, 2015; Terns and Terns, 2014). Based on SpCas9, new technologies such as base editors and prime editors enable the site-specific conversion of one or several DNA base pairs from one into another (Anzalone et al., 2019; Gaudelli et al., 2017; Komor et al., 2016). These new tools have brought about great interests in developing new therapeutics, and as most genetic disorders are caused by point mutations and small deletions/insertions, correcting these mutations is the most effective way to cure. Due to the inflexibility of mutated sites, base editors and prime editors are limited to a restrictive editing window. Therefore, the PAM requirement has become a major barrier to identify efficient gRNAs. In order to increase the targeting range of SpCas9, several studies have used protein engineering strategies to relax the PAM to NG or RY (R = A or G, Y = C or T) (Collias and Beisel, 2021; Hu et al., 2018; Nishimasu et al., 2018; Richter et al., 2020; Walton et al., 2020), which collectively only cover ~56% of sequences (Collias and Beisel, 2021). In addition to protein engineering, mining natural orthologs have also identified a collection of Cas proteins with different PAMs (Chatterjee et al., 2018, 2020; Collias and Beisel, 2021; Gasiunas et al., 2020). Although these variants have a certain effect on expanding the targeting scope of Cas proteins, the targets carrying most non-PAMs are still a limitation of efficient genome editing.

Here, we identified two new type II-C Cas9 enzymes from thermophiles *Alicyclobacillus tengchongensis* (*A. tengchongensis*) and *A. hesperidum*, with a very relaxed PAM CNNN and RNNA (R = A or G) for AtCas9 and GNNA for AhCas9 at their optimal temperature (55°C). Surprisingly, these two Cas9 enzymes exhibited near-PAMless cleavage toward physiologically negatively supercoiled dsDNA, with up to 95% cleavage when presented with mutant PAM supercoil but no cleavage toward the linear counterpart. More importantly, we found the thermophilic AtCas9 is active in mammalian cells with low off-target effects and shows near-PAMless cleavage of supercoil plasmids in *Escherichia coli* (*E. coli*).

RESULTS

In vivo and *in vitro* PAM identification for AtCas9 and AhCas9 showed no PAM preference toward negatively supercoiled DNA

The thermo-acidophilic bacterium *A. tengchongensis*, originally isolated from the sediment in a hot spring, can grow in a wide temperature range of 30°C–65°C (Kim et al., 2014). Analyzing the whole-genome sequence using CRISPR Finder (Couvin et al., 2018), we found that *A. tengchongensis* carries an intact CRISPR locus that includes the three Cas genes *cas9*, *cas1*, and *cas2* and the adjacent CRISPR array (Figure S1A). We purified AtCas9 and performed a biochemical analysis using one original spacer 21a from the CRISPR locus (Figures S1B and S1C). When guided by its cognate crRNA and tracrRNA, AtCas9 is able to cleave target DNA in the presence of Mg^{2+} at a pH and temperature that widely range from pH 5 to 8 and 37°C to 65°C, respectively (optimal activity at pH 6–8 and 55°C–60°C) (Figure S1C).

To identify the PAM for AtCas9, we constructed a PAM library plasmid containing 8 base pairs of randomized nucleotides adjacent to the protospacer 21a and performed transformation assays in *E. coli* harboring AtCas9 locus with the matching spacer 21a. This is an *in vivo* negative screen for PAM, as uncleaved plasmids are enriched upon antibiotic selection (Jiang et al., 2013). To our surprise, sequencing of survival plasmids exhibited no PAM preference in AtCas9-expressing *E. coli*, whereas the positive control SpCas9 showed a classic NGG PAM, consistent with previous reports (Jinek et al., 2012; Figure 1A). To rule out the possibility that AtCas9 is not active in mesophilic *E. coli*, we monitored cell growth as cleaved plasmid cannot replicate, and cells die upon antibiotic selection. Compared with control cells that either do not express AtCas9 or have a mismatched plasmid, cells that transformed with the matched PAM library plasmid or a known cleavage plasmid exhibited compromised cell growth (Figure 1B), indicating that AtCas9 is active in *E. coli*. Since the *in vivo* PAM screen did not identify the PAM sequence, we turned to the *in vitro* positive screen by sequencing the cleaved PAM library (Karvelis et al., 2015). We first treated the PAM library plasmid with restriction enzymes

Figure 1. *In vivo* and *in vitro* PAM identification for AtCas9 and AhCas9 show no PAM preference toward negatively supercoiled DNA

(A) *In vivo* PAM identification by AtCas9 (top) and SpCas9 (bottom). Frequency of individual base at each position was shown.

(B) Cleavage of plasmid substrates in *E. coli* cells and cell densities (OD_{600}) was measured every hour. Values and error bars reflect mean ± SD. n = 3.

(C) Schematic representation of PAM library plasmids carrying the 21a protospacer and an 8-nt randomized PAM sequence. Three DNA topoisomers generated with indicated restriction enzyme were tested for *in vitro* cleavage.

(D) Schematic diagram of AtCas9 domain structure (top) and the cleaved products resolved by agarose gel (bottom). dAtCas9 (D8A H617A N640A) is a catalytic inactive control. BH, bridge helix; REC, recognition lobe; L, linker; WED, wedge domain; TOPO, topoisomerase-homology domain; CTD, C-terminal domain.

(E) Quantification of cleavage efficiency. n = 3.

(F and G) Sequence logos and PAM wheel plots for AtCas9 and AhCas9 using two spacers 21a and 21b. Neg.sc, negative supercoil; OC, open circle.

(H) *In vitro* cleavage of WT (CATA) or mutated PAM (TATA) substrates in different topology. Controls include components minus one, a mismatch crRNA, or dAtCas9.

(I) *In vitro* cleavage of single-stranded DNA (ssDNA).

BsaI or Nt.BspQI to generate linear or open circle (OC) topoisomers for comparison with the negatively supercoiled plasmid (Figure 1C), the latter being used in the *E. coli* PAM screen. Three DNA isomers were incubated with AtCas9 in the presence of matched crRNA and tracrRNA, and digested products were analyzed on agarose gel (Figure 1D). Interestingly, up to 97% of the supercoiled PAM library was cleaved, whereas only 60% linear or OC isomers were digested at AtCas9's optimal temperature (Figures 1D and 1E). By introducing three mutations, one in RuvC and two in HNH nuclease domain (D8A H617A N640A), we generated catalytically dead AtCas9 (dAtCas9), which did not cleave linear, OC, or supercoiled isomers (Figure 1D), suggesting that the near-complete cleavage of supercoiled isomers requires the nuclease activity of AtCas9. Similar trends were observed when a different spacer and its PAM library substrate were used (Figure S2A). The near-complete cleavage of the negatively supercoiled PAM library explains why the *in vivo* PAM screen using supercoiled plasmid failed to identify any PAM preference. To map the PAM, we sequenced the input PAM library and the digested fragments. Up to 99.5% PAM combinations were present and relatively uniform, as revealed by quarterly distributed nucleotides in the PAM wheel or sequence logo (Figure S3A). To accurately present the PAM for AtCas9, we used sequence logos (Crooks et al., 2004) and the PAM wheel Krona plot (Leenay et al., 2016) to display the preference of individual nucleotides at each position and the nucleotide combinations. Using two different spacers with their respective protospacer substrates, we found AtCas9 has no preference at positions 1–4 but has a preference of C or A or G at position 5 when the substrates are linear or OC dsDNA (Figures 1F, 1G left, and S3B). By contrast, the preference is completely abolished when AtCas9 was incubated with negatively supercoiled dsDNA (Figures 1F and 1G). Under more stringent conditions, including incubation at a suboptimal temperature of 37°C or decreased enzyme-to-substrate ratio, a strong preference of C at position 5 and a small bias toward A at position 8 were associated with linear DNA, whereas no strong preference was observed in the supercoiled substrate (Figures S3C and S3D).

We next tested whether DNA topology-guided near-PAMless cleavage is shared by other Cas9 orthologs. Phylogenetic analysis based on 16S rRNA sequences indicated that *A. hesperidum* shares a 95% similarity with *A. tenchongenous* (Figure S2B). We then purified AhCas9 protein and performed *in vitro* PAM identification using two different spacers toward three DNA topoisomers. Similar to AtCas9, AhCas9 exhibited a PAM preference of NNNNGNNA (N_4GNNA) toward linear and OC isomers but no preference toward negatively supercoiled DNA (Figures 1F, 1G, and S2C).

Compared with other Cas9 orthologs, AtCas9 has the most relaxed PAM with a preference of C, A, or G at position 5 when the substrate is linear or OC dsDNA. Mutating PAM from CNNA to TNNA for AtCas9 or from GNNA to TNNT for AhCas9 completely abolished cleavage activity against linear dsDNA, confirming the requirement of PAM recognition and binding to initiate DNA unwinding and subsequent cleavage (Figures 1H and S2D). By contrast, up to 91% cleavage of negatively supercoiled dsDNA was observed when PAM was mutated (Figures 1H and S2D). In addition, catalytic inactive dAtCas9 RNP or wild-type RNP (WT RNP) complex with mismatched crRNA failed to cleave the substrates, suggesting that the topology-dependent cleavage of mutant PAM required the presence of tracrRNA, a matched crRNA, and the nuclease activity of Cas9 (Figures 1H and S2D). We then digested the cleaved products with a restriction enzyme NcoI to determine whether AtCas9- or AhCas9-mediated cleavage is site specific or not. Regardless of WT or mutant PAM, AtCas9- and AhCas9-cleaved products exhibited two specific bands post NcoI treatment, suggesting that topology-guided mutant PAM cleavage via AtCas9 and AhCas9 is site specific (Figure S2E). Some Cas9 orthologs also exhibited cleavage activity against single-stranded DNA (ssDNA), and this function is gRNA dependent but PAM independent (Zhang et al., 2015). To rule out the possibility that the cleavage of mutant PAM is a consequence of ssDNA activity, we incubated AtCas9 RNP with complementary ssDNA and found that AtCas9 is able to cleave ssDNA without the need of tracrRNA (Figure 1I). By contrast, the cleavage of dsDNA requires the presence of both crRNA and tracrRNA, arguing against the possibility that the mutant PAM cleavage is a result of its ssDNA cleavage activity. Collectively, these observations suggest that DNA topology plays an important role in facilitating Cas9 cleavage of mutant PAM dsDNA, and negatively supercoiled isomers could promote effective cleavage when presented with a matched crRNA and tracrRNA.

Naturally occurring underwound DNA is able to initiate dsDNA cleavage in a crRNA-matched manner

DNA topology plays an essential role in orchestrating genome structure and gene transcription (Kuzminov, 2018). In order to save space in mesophilic and thermophilic bacteria, DNA is wrapped as a negative supercoil when the right-handed double-helix DNA is twisted in a left-handed fashion, which preferentially underwinds the DNA helix (Ivanov et al., 2020). In extreme thermophiles, in order to protect genome stability from high-temperature melting, DNA is wrapped as a positive supercoil, which involves twisting in a right-handed orientation, resulting in overwinding of the helix and the generation of positive torsional strain (Bustamante et al., 2003). During transcription, the formation of the R-loop between RNA polymerase and DNA duplex generates positive supercoils ahead of the transcription and negative supercoils behind the transcription (Chong et al., 2014). To determine how torsional strain regulates AtCas9 activity, we generated different levels of positively supercoiled DNA by treating negatively supercoiled DNA with reverse gyrase and validated the preparation (Figure S4A). Similar to linear DNA, mutating PAM from C to T completely abolished AtCas9 activity against positively supercoiled substrates (Figures 2A and S4B). As positive torsional strain increased, a trend in decreased Cas9 activity was noticed in WT PAM, and this phenomenon was more obvious at 37°C (Figure 2A). Sequencing of PAM showed that in addition to a position 5 preference, the positive supercoil isomer has a small preference for A at position 8, similarly to *in vitro* cleavage under stringent conditions (Figure 2B). These data suggest that the negative torsional strain residing in negatively supercoiled isomers strongly promotes the activity of AtCas9, whereas a positive strain in positively supercoiled DNA represses AtCas9 activity.

Please cite this article in press as: Shi et al., DNA topology regulates PAM-Cas9 interaction and DNA unwinding to enable near-PAMless cleavage by thermophilic Cas9, Molecular Cell (2022), https://doi.org/10.1016/j.molcel.2022.09.032

CellPress

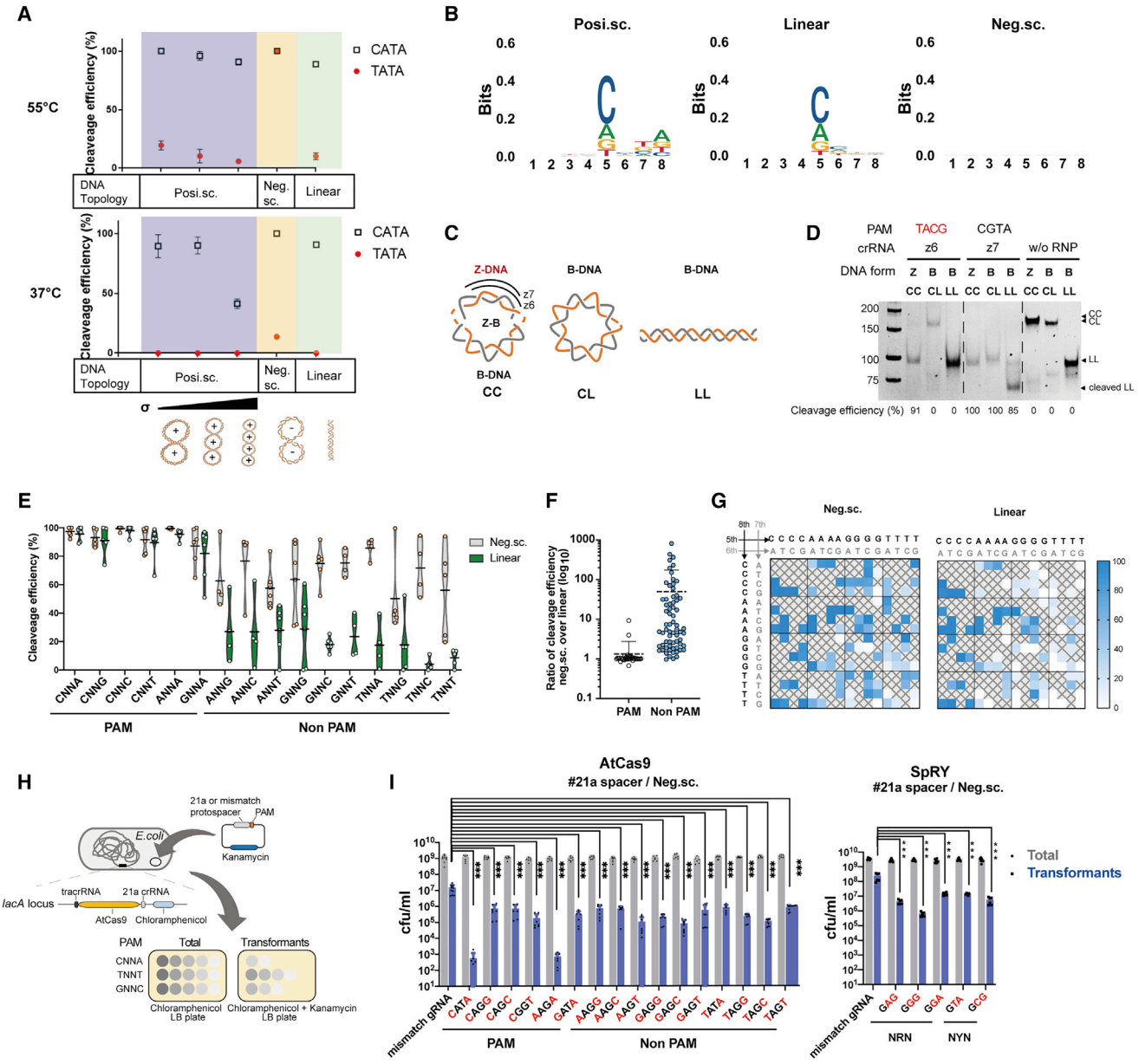

Figure 2. Near-PAMless cleavage of underwound dsDNA both *in vitro* and in *E. coli*

(A) Quantification of *in vitro* cleavage of three dsDNA topoisomers: positive supercoil, negative supercoil, and linear (also see Figure S4B). Data are presented as mean ± SD, n = 3. Posi.sc, positive supercoil; Neg.sc, negative supercoil; WT PAM, CATA; mutant PAM, TATA.

(B) Sequence logo plot of PAM sequences for three topoisomers.

(C) Schematic of *in vitro* prepared Z-DNA and B-DNA isomers. CC, a chimeric circular DNA containing both Z-form and B-form; CL, a B-form open circle isomer; LL, a B-form linear isomer. z6 and z7 represent two spacers.

(D) *In vitro* cleavage of Z-form dsDNA with mutated PAM or WT PAM. w/o RNP, without RNP.

(E) Cleavage of negative supercoil and linear dsDNA with indicated PAMs. Each dot represents a different spacer, and the NNs in PAMs are different, indicating a mixed sequence. Data are presented as mean.

(F) Comparison of cleavage efficiency between negative supercoil and linear dsDNA. Data are grouped according to PAM and non-PAM substrates.

(G) Heatmap representation of combined mean cleavage efficiency of PAMs.

(H) Schematic of natural transformation assays in *E. coli*. A mini AtCas9 CRISPR locus bearing 21a spacer was inserted into *lacA* locus. AtCas9-expressing *E. coli* was transformed with plasmids of 16 PAMs bearing complementary sequence to 21a spacer or a mismatch EGFP control.

(I) Quantification of colony-forming units (CFU)/mL is shown for total cells (gray bars) and kanamycin-resistant (blue bars) transformants, n = 6. Student's t test is performed. ***p < 0.0001.

In mammalian cells, DNA has three major topological forms, that is, the B-form, Z-form, and A-form. The B-form is the most abundant and stable right-handed double helix, whereas the Z-form is a less stable left-handed double helix with underwound structure (Herbert, 2019). Z-DNA is usually composed of alternating purines and pyrimidines and tends to form in eukaryotic cells ahead of the transcription active site (Rich and Zhang, 2003; Oberstrass et al., 2012). To determine whether AtCas9 is able to cleave mutant PAM in Z-DNA isomers, we engineered an 89-nt B-Z hybrid mini-circle DNA as previously reported (Zhang et al., 2019; Figures 2C and S4C) and performed *in vitro* cleavage using crRNA that matches the Z-DNA region. Similar to negatively supercoiled isomers, Z-DNA bearing mutated PAM was cleaved by AtCas9 with an efficiency of 91% (Figure 2D). Collectively, by comparing different topoisomers, we showed that AtCas9 is able to cleave naturally occurring underwound DNA, such as negatively supercoiled plasmid and Z-DNA, and that the cleavage is PAM independent.

Near-PAMless cleavage of negatively supercoiled plasmids both *in vitro* and in *E. coli*

Our deep sequencing suggested that AtCas9 has no PAM preference against negatively supercoiled topoisomers, based on two sgRNAs (Figure 1F). To determine whether topology-guided near-PAMless cleavage is shared by other sgRNAs, we tested a total of 82 gRNAs with 16 PAM combinations differing in positions 5 and 8, and two topoisomers (linear and negative supercoil) were compared. When presented with linear dsDNA, AtCas9 showed a canonical PAM CNNN and RNNA (R = A or G), with an average efficiency of 91.7% of 34 gRNAs tested (Figure 2E). Non-PAM combinations such as RNNB (B = non-A, R = A/G) and TNNN exhibited a median efficiency of 20% in linear dsDNA, indicating that these sequences are less likely to be recognized by AtCas9 when presented as B-DNA. When incubated with negatively supercoiled dsDNA, PAM preferences extended to almost all non-PAM combinations except TNNG (Figure 2E), with a combined median efficiency of 80%. By direct comparison of two topoisomers of each gRNA, we found that in non-PAM substrates, negative supercoil greatly enhances cleavage efficiency by an average of 50-fold over linear isomer, whereas a minor 1.3-fold increase of negative supercoil over linear isomer is observed in PAM-containing substrates (Figure 2F). When plotting the PAM combinations and their respective cleavage efficiency on heatmaps (Gao et al., 2017), negatively supercoiled plasmid exhibited broader tolerance of PAM combinations than linear DNA when incubated with AtCas9 (Figure 2G).

To determine whether the topology-dependent near-PAMless cleavage holds the case *in vivo*, we tested the editing of 16 PAMs individually in *E. coli*. A minimal AtCas9 locus including Cas9, tracrRNA, and a repeat-spacer array was introduced into the *lacA* locus in *E. coli* (Figure 2H). We then transformed plasmids encoding a matching protospacer with indicated PAMs. Comparing with mismatch control or dAtCas9 control, all 16 PAMs showed a ~10- to 10,000-fold decrease in colony formation, indicating that AtCas9 is able to cleave supercoiled plasmid in all 16 PAM combinations (Figures 2I and S4D). Notably, a higher cutting efficiency was observed when PAM is CNNA and ANNA, suggesting that DNA topology and PAM sequence together determine the final cleavage activity of AtCas9. SpRY Cas9 is an engineered Cas9 variant with relaxed PAM of NRN and NYN (R = A and G, Y = C and T) (Walton et al., 2020). To compare the PAM tolerance with AtCas9, we engineered an *E.coli* strain to stably express SpRY, tracrRNA, and a repeat-spacer array. SpRY-expressing *E.coli* was transformed with matched substrates bearing 16 PAMs. While the PAM combinations tested exhibited a ~10- to 100-fold decrease in colony formation (Figure 2I), the cleavage efficiency with its optimal PAM (NGG) was much lower than that of AtCas9 (CNNA or ANNA). Together, our data strongly suggest that AtCas9 has a relax PAM of CNNN and RNNA (R = A or G) and is able to perform near-PAMless cleavage of underwound DNA both *in vitro* and in *E. coli*.

DNA topology regulates PAM-Cas9 interaction and DNA unwinding to enable cleavage of dsDNA with mutant PAM

Dissecting how DNA topology affects the cleavage of dsDNA, we investigated the effect of topology on regulating Cas9 binding. Electrophoretic mobility shift assay (EMSA) was used to measure the binding affinities of pre-complexed RNP to different topoisomers. Unlike SpCas9 or NmeCas9 (Ma et al., 2015; Rousseau et al., 2018), the binding of AtCas9 with Cy5-labeled oligonucleotides depends on the presence of magnesium, and this binding is crRNA dependent (Figure 3A). Investigating which part of the ternary complex are affected by magnesium ions, we fluorescently labeled two components with different colors and performed the binding assay. In the absence of magnesium, crRNA still formed a complex with dAtCas9, albeit at higher doses (Figure S5A), whereas little interaction was observed between tracrRNA and dAtCas9 (Figure S5B), indicating that the formation of tracrRNA-crRNA-dAtCas9 complex requires magnesium. Using the same spacer, we found that AtCas9 was able to bind mutant PAM in B-form, although at a higher dose (Figures 3B and S5C), whereas SpCas9 control showed no binding when PAM is mutated (Figures 3C and S5D). To mimic underwound DNA in the linear isomer, we introduced a two-base bulge in the non-target strand (NTS) strand of the mutant PAM substrate (Figure 4C), which theoretically lowers the energy required to unwind dsDNA. Introducing a two-base bulge in the mutant-PAM substrate greatly enhanced the binding affinities to levels comparable to that of WT PAM substrate (Figures 3B and S5C). We then labeled negatively supercoiled plasmid or linear plasmid with fluorescent dye, incubating it with dAtCas9 RNP. In line with oligonucleotides EMSA, although the linear isomer bearing a mutated PAM was able to bind dAtCas9, it has a higher KD ± SD of 89.12 ± 21.46 nM compared with the 35.17 ± 0.44 nM of WT PAM (Figures 3D and S5E). Negatively supercoiled isomers exhibited stronger binding affinity than their linear counterparts, with a KD ± SD of 21.74 ± 2.74 nM and 28.96 ± 6.25nM when presented with WT PAM and mutant PAM, respectively (Figure 3D). In line with the binding assay, cleavage kinetic analysis using two different spacers showed that AtCas9 had robust cleavage activities against negatively supercoiled DNA with mutant PAM (Figures 3E and S6A–S6C).

Please cite this article in press as: Shi et al., DNA topology regulates PAM-Cas9 interaction and DNA unwinding to enable near-PAMless cleavage by thermophilic Cas9, Molecular Cell (2022), https://doi.org/10.1016/j.molcel.2022.09.032

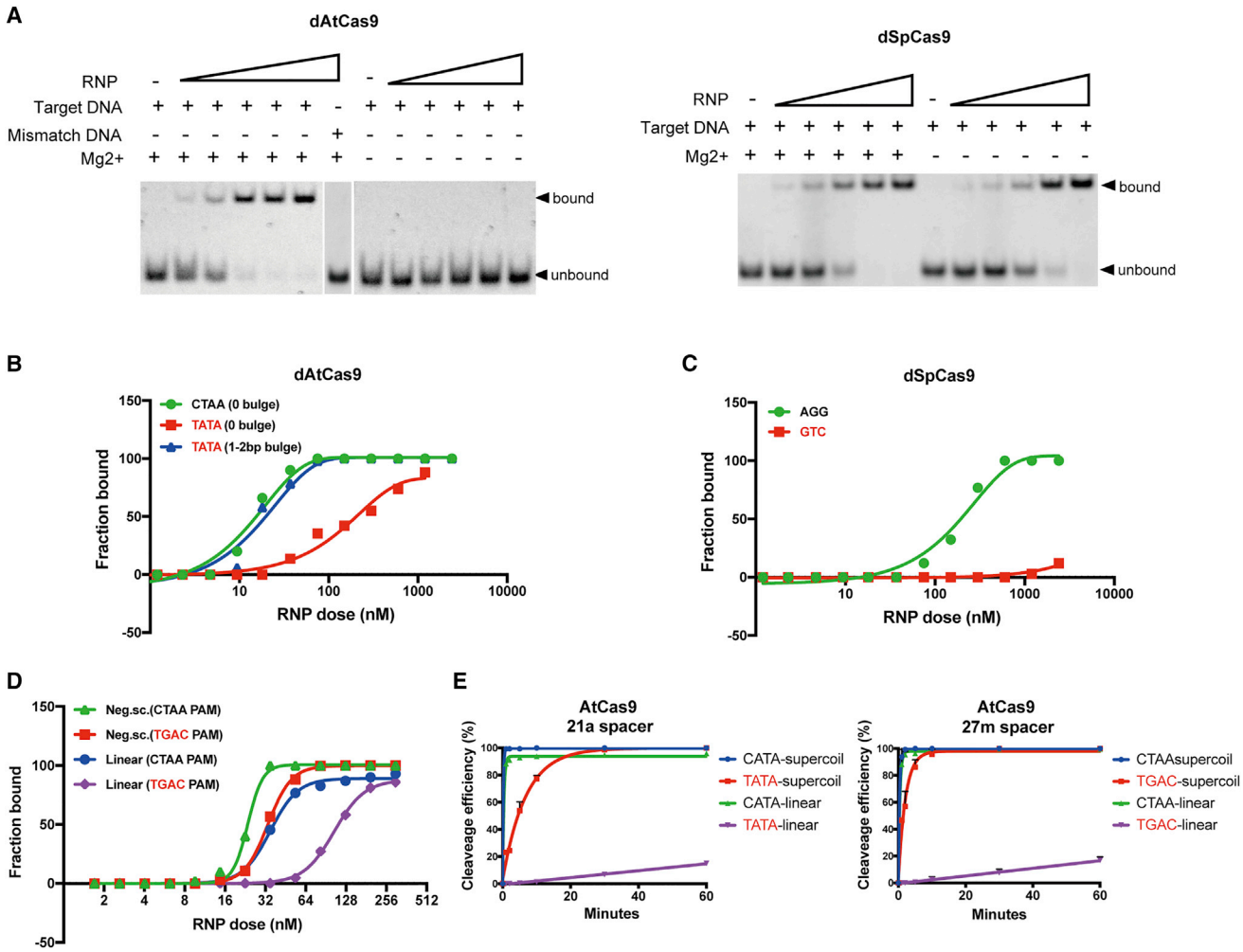

Figure 3. AtCas9 has higher binding affinity and cleavage kinetics toward underwound dsDNA with mutated PAM

(A) Electrophoretic mobility shift assay (EMSA) were carried out by incubating dAtCas9 RNP (left) or dSpCas9 RNP (right) with Cy5-labeled oligonucleotides (50 bp) in the presence or absence of Mg^{2+}.

(B and C) Quantification of EMSA with dAtCas9 RNP (B) or SpCas9 RNP (C) at their optimal temperatures (also see Figures S5C and S5D). WT PAM, mutant PAM, or bulge DNA was indicated as green, red, or blue, respectively. The equilibrium dissociation constant for AtCas9 is 18.32 ± 6.8 nM, 158.3 ± 7.9 nM, or 22.62 ± 7.2 nM for WT PAM, mutant PAM, or mutant PAM with 2-nt bulge, respectively. The KD of SpCas9 with WT PAM is 189.9 nM, and no binding is observed in mutant PAM.

(D) Higher binding affinity of AtCas9 RNPs toward negative supercoil than linear dsDNA. WT PAM (CTAA) or mutant PAM (TGAC) were tested. KD ± SD for negative supercoil is 21.74 ± 2.74 nM and 28.96 ± 6.25 nM for WT PAM and mutant PAM, respectively. KD ± SD for linear is 35.17 ± 0.44 nM and 89.12 ± 21.46 nM for WT PAM and mutant PAM, respectively (also see Figure S5E).

(E) Kinetic analysis of cleavage efficiency using the two different crRNAs 21a and 27m on WT (black) or mutant PAM (red) under different topology (also see Figure S6). n = 3, and data are fitted with non-linear regression for entire figure.

Previous studies have shown that among the many factors that regulate Cas9 activity, PAM recognition and subsequent DNA unwinding are the primary determinants (Gong et al., 2018; Sternberg et al., 2014). It is possible that DNA topology acts through facilitating the DNA unwinding process or regulating PAM recognition or both. To rule out the influence of DNA unwinding, we performed competition experiments using competitors that harbor a series of repetitive mutant PAM sequences without the matched protospacer (Figure 4A). By monitoring the cleavage of the 6-Carboxyfluorescein (FAM)-labeled, matched substrate carrying WT PAM, we could infer whether topologically different PAM mutants were able to compete for AtCas9 binding. Negative supercoil competitors substantially reduced the cleavage of the FAM-labeled substrates, compared with the linear isomer (Figures 4B and S7A), indicating that the residence time of Cas9-RNA on negatively supercoiled competitor DNA is longer than on the linear isomer. This result persisted over a range of competitor DNA concentrations, suggesting that the residence time of Cas9-RNA on non-target negative supercoil DNA lacking PAMs and protospacer is non-negligible, and DNA topology could affect the ability of RNP complex in sampling DNA even when PAM is lacking.

Please cite this article in press as: Shi et al., DNA topology regulates PAM-Cas9 interaction and DNA unwinding to enable near-PAMless cleavage by thermophilic Cas9, Molecular Cell (2022), https://doi.org/10.1016/j.molcel.2022.09.032

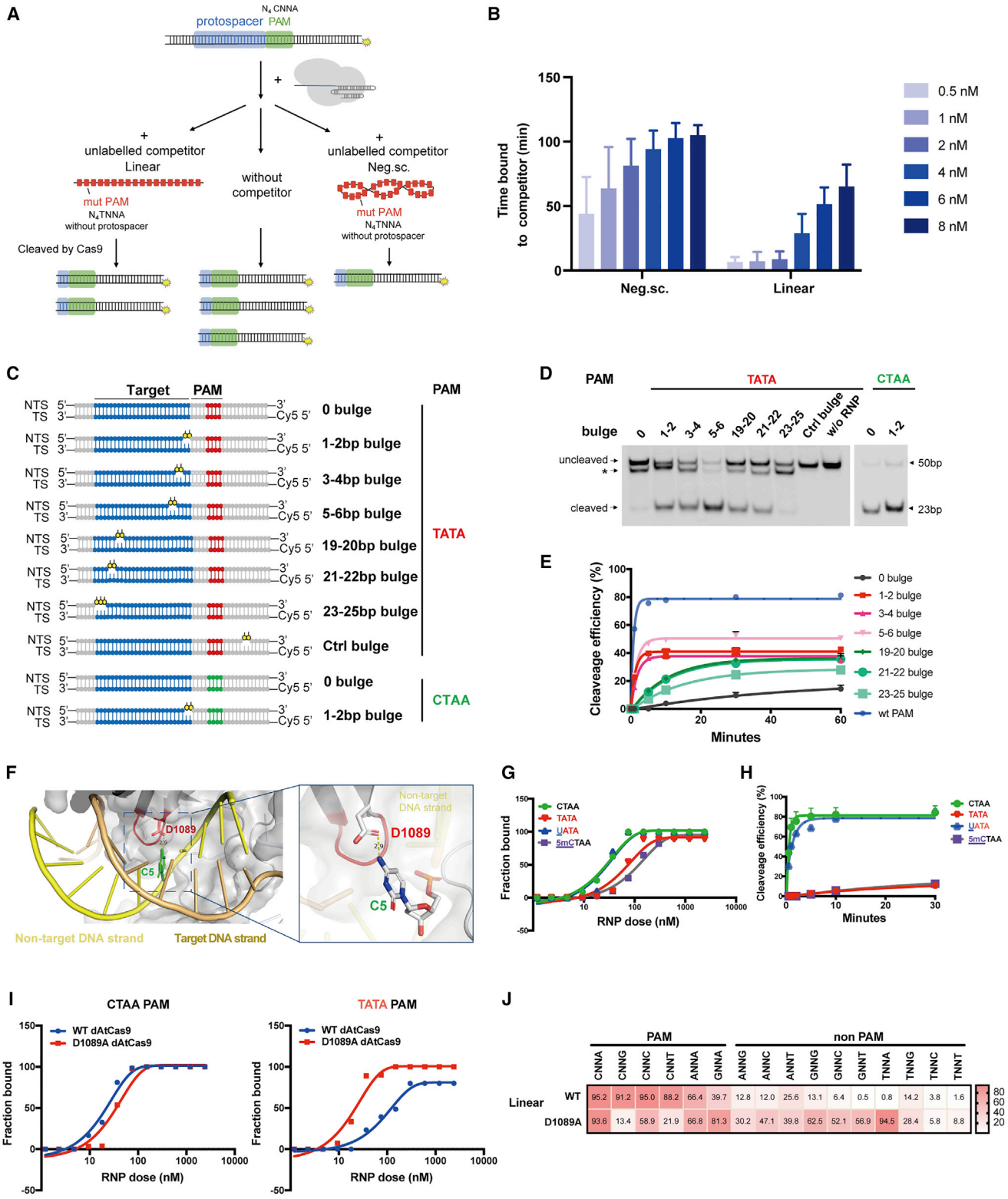

Figure 4. Underwound topology facilitates AtCas9 and non-PAM substrate binding and the unwinding process

(A) Schematic of the competition cleavage assay. AtCas9 RNP complex was incubated with FAM-labeled oligonucleotides bearing the complementary protospacer 27m with WT PAM (CTAA). Unlabeled topoisomers bearing repetitive mutant PAMs were the competitors.

(B) Quantification of competition assay (also see Figure S7A, mean ± SD, n = 3).

(legend continued on next page)

Please cite this article in press as: Shi et al., DNA topology regulates PAM-Cas9 interaction and DNA unwinding to enable near-PAMless cleavage by thermophilic Cas9, Molecular Cell (2022), https://doi.org/10.1016/j.molcel.2022.09.032

DNA duplex unwinding can be regulated by negative or positive torsional strain (Bustamante et al., 2003). We then reasoned that the negative torsional strain presented in underwound DNA could also facilitate the DNA unwinding process. To test this hypothesis, we generated a series of bulged oligonucleotides with two-base mismatches in the NTS spacing away from the PAM (Figure 4C), which mimic underwound DNAs. Consistent with our expectation, a two-base mismatch in the linear dsDNA target was sufficient to enhance AtCas9's cleavage in mutant PAM (Figure 4D). To rule out the possibility that a two-base bulge may have an impact on the overall DNA topology in a 50-nt oligonucleotide, we synthesized a longer 120-nt oligonucleotide and performed a kinetic analysis. In concert with short oligonucleotides, AtCas9 exhibited up to a 30-fold increase of cleavage toward mutant PAM dsDNA bearing a 2-nt bulge, compared with control (Figures 4E and S7B). Although DNA bulge could enable the cleavage of mutant PAM, the cleavage kinetics is much slower than that of WT PAM control, indicating that the DNA-torque-regulated DNA unwinding process partially contributes to the cleavage of mutant PAM dsDNA. Thus, DNA topology could regulate both Cas9-PAM interaction and DNA unwinding to enable effective cleavage of mutant PAM dsDNA.

The ability of AtCas9 to bind with mutant PAM suggests that other than base-pairing-mediated hydrogen bond interaction, other mechanisms might exist to facilitate PAM-Cas9 interaction. We used two methods, AlphaFold2 and SWISS-MODEL, to simulate a predictive AtCas9 structure and noticed that in the PI region, a β sheet-loop-β sheet motif of Atcas9 RNP is closely accommodated into the major groove of the double helix (Figures 4F and S7C), likely serving as an anchoring point to support the Cas9-DNA interaction. Detailed analysis identified that the side chain of Asp1089 (D1089) was in proximity to the C5 on non-target DNA strand, and they were able to form a hydrogen bond interaction, leading to a strong binding affinity with C5 in the 5′-N_4CNNN-3′ PAM (Figure 4F). AtCas9 has a promiscuous PAM of A/G/C at position 5 and is resistant to thymine (T). Compared with the other nucleotides, thymine is the only nucleotide with a methyl group. It is possible that a steric clash could occur between the methyl group of thymine and the side chain of Asp1089. In support, substitution of thymine with uracil (U)—the latter lacks the methyl group—strongly promotes the binding and cleavage activity, whereas addition of a methyl group at C5 greatly diminishes the binding and cleavage of AtCas9 (Figures 4G, 4H, S7D, and S7E). Conversely, mutating Asp1089 to Ala1089—the latter of which has a smaller side chain—showed enhanced binding affinity to thymine (T5) (Figures 4I and S5F) and increased cleavage efficiency against non-PAM substrates (Figure 4J). Together, these data reveal that the unique protein-PAM interaction pattern and the effect of DNA topology function jointly to determine the ultimate substrate cleavage activity of AtCas9.

Genome-editing activity of AtCas9 in mammalian cells

To determine whether the thermophilic AtCas9 is active in mammalian cells, we codon-optimized the AtCas9 and compared different nuclear localization signals (NLSs) to ensure nuclear delivery in mammalian cells (Figure 5A). A dual NLS (cmyc-nucleoplasmin) was selected and sgRNA driven by U6 promoter was tested for cleavage in two different 293T reporter cell lines. One has a single-copy EGFP and the other reporter has a truncated p53 sequence followed by a 1-bp frameshift EGFP, as loss-of-signal or gain-of-signal reporter, respectively. sgRNAs targeting EGFP or p53 were designed and transfected into corresponding cell lines. EGFP disruption or activation was analyzed by fluorescence-activated cell sorting (FACS) and amplicon sequencing (next-generation sequencing [NGS]) to measure the editing efficiency. First, we optimized the spacer length by transfecting various lengths of spacer targeting p53 and EGFP locus, and we tested three spacers for each locus (Figures 5B–5D and S8A–S8F). Based on a summary of 6 spacers, we found that AtCas9 has a high editing efficiency when the spacer length ranges from 21 to 24 nt (Figure 5B). When spacer length is 22 nt, a slightly higher mean editing efficiency is observed. Moreover, of the six gRNAs tested, the 22-nt length exhibited the most stable and consistent high editing (Figures 5C, 5D, and S8A–S8F). Therefore, when using AtCas9 for genome editing, 22 nt can be the preferred spacer length, and the optimal spacer length for a specific gRNA can be further tested. Second, we engineered the sgRNA scaffold by extending the stem-loop 1 with a bulge structure, according to the NmeCas9 sgRNA structure, or truncating the repeat-anti-repeat and stem-loop 2 region (Figure 5E). By designing two sgRNAs targeting the EGFP locus, we found that truncating the repeat-anti-repeat and extending stem-loop 1 with an additional bulge structure (203 construct) led to a 3.4-fold increase in EGFP disruption, compared with WT (200 construct). Truncating the repeat-anti-repeat and stem-loop 2 region (202 construct) did not further enhance editing (Figures 5E and 5F). Thus far, we have optimized AtCas9 and its gRNA to

(C) Illustration of DNA bulge substrates recapitulating underwound dsDNA. Target sequence is labeled blue, mutant PAM (TATA) or WT PAM (CTAA) is labeled red or green, respectively. A 2- to 3-nt-length bulged DNA is generated by mutating the NTS highlighted in yellow. TS, target strand; NTS, non-target strand.
(D) *In vitro* cleavage assay of Cy5-labeled DNA (50 bp) bearing indicated bulges. w/o, without. *indicated nicked products.
(E) Kinetic analysis of cleavage efficiency using 120-bp bulged substrates with WT or mutant PAM (see Figure S7B).
(F) AlphaFold2 simulated AtCas9-RNA-dsDNA structure. In the PAM-interacting region of AtCas9, a β sheet-loop-β sheet motif docked into the major groove of target DNA. Distance between the side chain of D1089 and C(−5)′ is 2.9 Å.
(G) EMSA of dAtCas9 in binding with different PAM variants: CTAA, TATA, UATA, and 5mCTAA (see Figure S7D). KD for dAtCas9 to PAM variants CTAA, TATA, UATA, and 5mCTAA are 24.89, 59.24, 25.8, and 106.5 nM, respectively.
(H) Cleavage of oligonucleotides bearing different PAMs (see Figure S7E).
(I) EMSA was performed with dAtCas9 or dAtCas9-D1089A RNP against cy5-labeled WT (CTAA) or mutant PAM (TATA) substrates (see Figure S5F). KD for dAtCas9 and dAtCas9-D1089A to WT PAM are 19.34 and 31.27 nM, respectively; KD ± SD for dAtCas9 and dAtCas9-D1089A to mutant PAM are 77.18 ± 11.54 nM and 25.03 ± 8.58 nM, respectively.
(J) *In vitro* cleavage of WT AtCas9 or D1089A-Cas9 on negative supercoil and linear DNA with different PAMs. Each PAM variant has at least two distinct spacer sequences, and mean value was plotted.

Please cite this article in press as: Shi et al., DNA topology regulates PAM-Cas9 interaction and DNA unwinding to enable near-PAMless cleavage by thermophilic Cas9, Molecular Cell (2022), https://doi.org/10.1016/j.molcel.2022.09.032

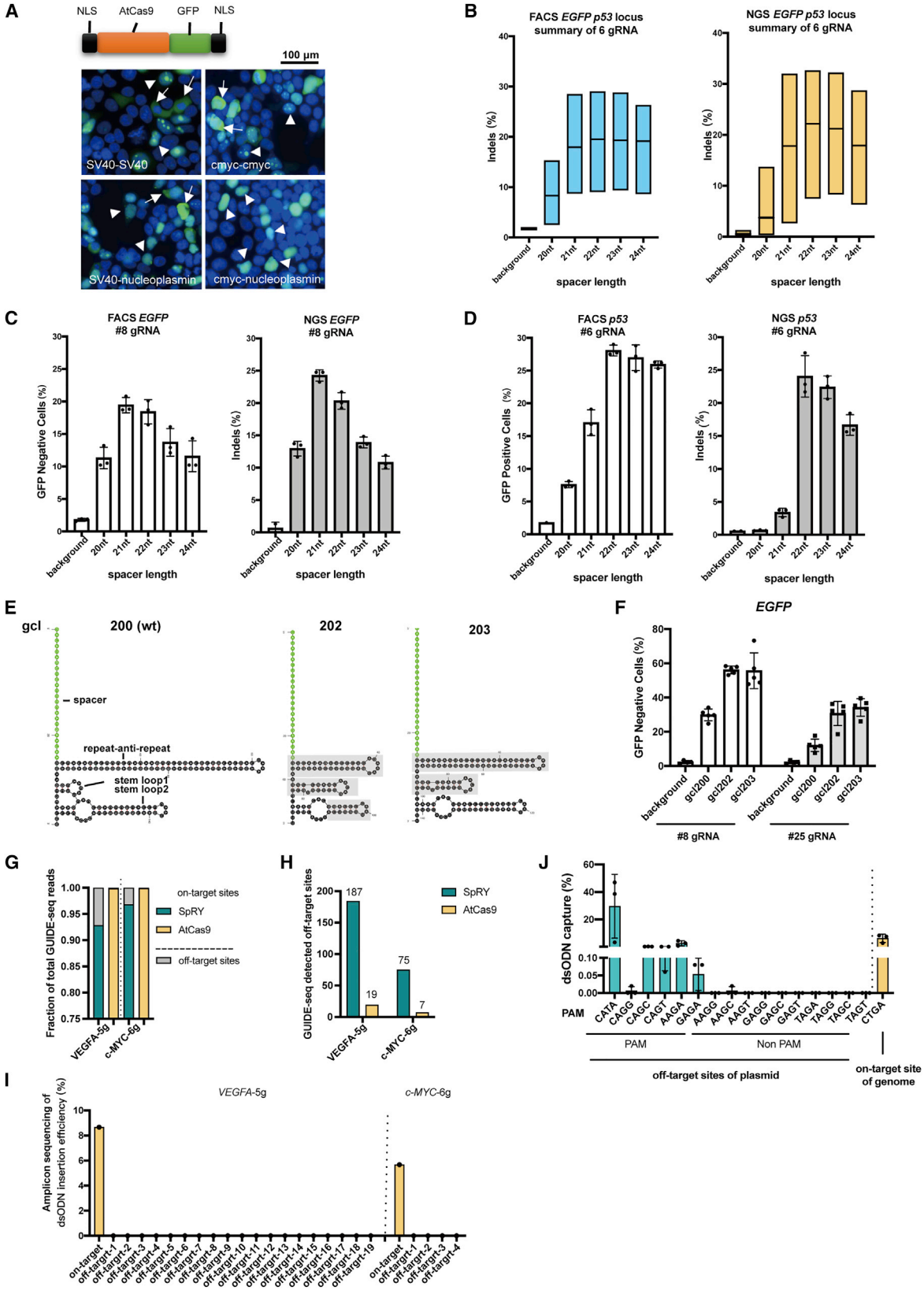

(legend on next page)

be able to achieve 60% efficiency at a lentivirus-generated EGFP locus.

Next, we examined the off-target effect of AtCas9 using genome-wide unbiased identification of DSBs enabled by sequencing (GUIDE-seq) (Tsai et al., 2015). By comparison with SpRY, we found that AtCas9 had a higher ratio of on-target integration to total editing events (Figures 5G, S9A, and S9B), and the number of off-target sites of AtCas9 was significantly lower (Figures 5H, S9A, and S9B). Amplicon sequencing further confirmed that the on-target double-stranded oligodeoxynucleotides (dsODN) integration was about 6%–8% while no sequencing read was detected at the off-target sites identified from GUIDE-seq in the two sites tested (Figure 5I), suggesting that AtCas9 is a high-fidelity genome-editing enzyme with no detectable off-target effect. To explore if the off-target profile of AtCas9 is regulated by its unique PAM interrogation modality, we co-transfected negatively supercoiled plasmid bearing matched protospacer with 16 different PAMs as potential off-target sites. By sequencing on-target integration sites on the genome and off-target sites on plasmids, we found that higher dsODN insertions were captured on plasmid bearing CNNA PAM when compared with the genomic on-target site (Figure 5J). When PAM is CNNH (H = non-G) and RNNA (R = A/G), detectable dsODN insertions were observed in plasmid substrate (Figure 5J). Together, these data indicate that AtCas9 is a high-fidelity enzyme with little off-target effect.

Considering high constraints of PAM selection for base editors (Hu et al., 2018; Komor et al., 2016; Nishimasu et al., 2018), we explored the application of AtCas9 in base editing. When co-transfecting AtCas9-expressing plasmid and negatively supercoiled substrates with 16 different PAMs, we found AtCas9-BE3 (D8A) is able to generate editing in 13 PAMs with variable efficiencies (Figure 6A). When presented with WT PAM (CNNN and RNNA), the combined efficiency reaches up to 46%. Consistent with *in vitro* data, D1089A AtCas9-BE3 has enhanced C-to-T editing efficiency in mutant-PAM substrates with a minor decrease in substrates carrying CNNN PAM. We next determined the C•G-to-T•A base-editing activities of AtCas9 in four different loci (*EGFP*, *VEGFA*, *RUNX1*, and *C-MYC*) and compared them with xCas9 and SpRY, two recently engineered Cas9 variants with relax PAM. Given that the PAM structure is different between SpCas9 variants (NNN) and AtCas9 (N_4CNNN, N_4RNNA), we kept the spacer sequence the same for comparison. We separately transfected plasmids encoding xCas9(3.7)-BE3, SpRY-BE3, and AtCas9-BE3 into mammalian cells to compare editing efficiency on all 25 sites (Figures 6B–6D). At the N_4CNNA PAM target sites tested, AtCas9-BE3 averaged 30.91% ± 2.7% C•G-to-T•A conversion, whereas xCas9-BE3 averaged 6.75% ± 0.72% and SpRY-BE3 averaged 24.66% ± 0.01% C•G-to-T•A conversion (Figures 6B–6D). At the N_4CNNG, N_4CNNC, N_4CNNT, and N_4ANNA PAM sites tested, AtCas9-BE3 averaged 16.58% ± 0.21% editing, whereas xCas9-BE3 or SpRY-BE3 resulted in 7.65% ± 1.07% or 18.12% ± 3.86%, respectively. Considering all gRNAs tested, AtCas9 showed a combined efficiency of 25.76% (Figure 6E), a ~3.7-fold increase compared with that of xCas9 and comparable activity with SpRY. Analyzing the editing windows in detail for all PAMs tested, we found AtCas9-BE3 has a broad editing window from positions 1 to 17 with peak editing from positions 5 to 14, which is different than SpRY (Figures 6F and 6G). We also determined the ability of AtCas9-ABE8e in A•T-to-G•C base editing at N_4CNNR and N_4ANNA PAM sites. Of the 41 gRNAs targeting four different loci tested, AtCas9-ABE8e exhibited an average efficiency of 16.72% ± 2.12%, ranging from 0.03% to 50.25% (Figures 6H and 6I). Similar to cytosine base editor, AtCas9-ABE8e can edit a wide range of adenine from positions 1 to 15 with a peak editing window from positions 5 to 13 (Figures 6J and 6K). Taken together, our data show that AtCas9 is able to mediate effective base conversion in the mammalian genome, and its broad PAM editing of underwound DNA has added a new tool to the genome-editing family.

DISCUSSION

For CRISPR-Cas9-mediated adaptive immunity, PAM plays critical roles in distinguishing self versus non-self (Marraffini and Sontheimer, 2010). In the current model of action, Cas9 recognizes PAM via sequence-dependent non-covalent bonding between Cas9 and target DNA (Anders et al., 2014). Although PAM sequence differs between orthologs, it is thought that this sequence-dependent protein-DNA interaction functions similarly for various Cas proteins, and non-PAM-containing sequences are unlikely to be bound by Cas effectors. Here, we identified a new thermophilic AtCas9, unlike other orthologs, which developed an unanticipated model of PAM interaction that can be robustly regulated by DNA topology (Figure 7). In the PI domain of AtCas9, a unique β sheet-loop-β sheet motif closely docked into the major groove of the double helix, serving as an additional anchoring point besides sequence-dependent interaction to initiate DNA unwinding. An analysis of the motif further identified that the side chain of Asp1089 was in close proximity to C5 in the N_4CNNN PAM, likely forming a hydrogen

Figure 5. Genome-editing activity of AtCas9 in mammalian cells

(A) Optimization of nuclear localization signals (NLSs) to enable nuclear import of AtCas9. Blue, nuclei; green, GFP; arrow, cytoplasmic localization; arrowhead, nuclear localization; scale bars, 100 μm.

(B) Summarized cleavage activity of six gRNAs with variable spacer lengths in two reporter cell lines by FACS (left) and amplicon sequencing (right).

(C and D) FACS analysis of cleavage efficiency by EGFP disruption (C) or EGFP activation (D).

(E) Schematic of AtCas9 sgRNA structures. Gray shading indicates the engineered domain.

(F) AtCas9 cleavage activity against EGFP locus with three gRNA scaffold variants.

(G) Fraction of on-target integration reads over total reads for AtCas9 and SpRY.

(H) Number of off-target sites for AtCas9 and SpRY using two different spacers.

(I) Amplicon sequencing of the potential off-target sites identified from GUIDE-seq.

(J) Off-target analysis of AtCas9 for negatively supercoiled plasmids with indicated PAMs by amplicon sequencing. Data are shown as mean ± SD. $n \geq 3$ for the entire figure.

Please cite this article in press as: Shi et al., DNA topology regulates PAM-Cas9 interaction and DNA unwinding to enable near-PAMless cleavage by thermophilic Cas9, Molecular Cell (2022), https://doi.org/10.1016/j.molcel.2022.09.032

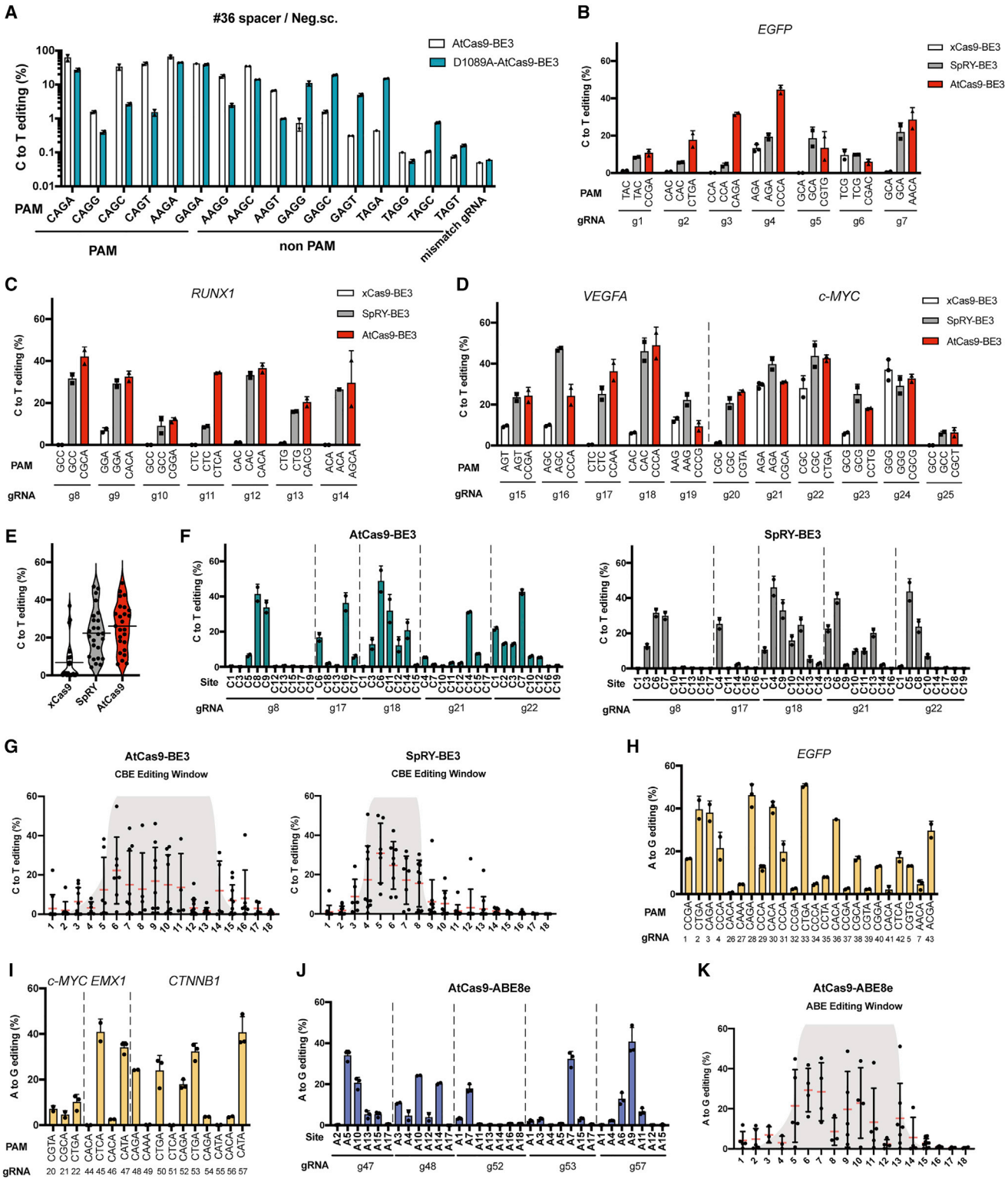

Figure 6. AtCas9 enables effective base editing in endogenous locus

(A) *In vivo* base editing of negatively supercoiled plasmids with indicated PAMs in HEK293T cells. Plasmids encoding wild-type AtCas9-BE3 or D1089A variant were co-transfected with plasmid encoding PAM variants.

(B–D) C-to-T base-editing efficiency of AtCas9, xCas9, and SpRY at four different loci (*EGFP*, *C-MYC*, *VEGFA*, and *RUNX1*) in 293T cells with indicated PAMs. AtCas9 and SpCas9 variants were compared by the same spacer at each site.

(legend continued on next page)

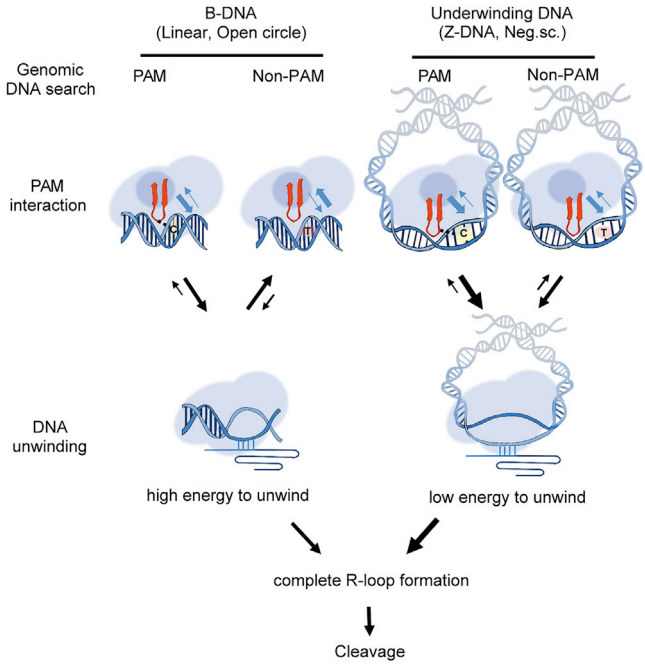

Figure 7. Model for topology-guided dsDNA cleavage of mutant PAM substrate

When Cas9 searches its target site on the genome, the difference in DNA topology could affect the PAM recognition and DNA unwinding processes. Similar to other Cas orthologs, AtCas9 recognizes its PAM through the formation of hydrogen bond with C5 in target DNA (highlighted in yellow). Besides this sequence-dependent recognition, the β sheet-loop-β sheet motif (marked in red) of AtCas9 closely docks into the major groove of dsDNA, serving as a second anchoring point to initiate the subsequent DNA unwinding. Underwound DNA such as negative supercoil and Z-DNA are structurally different than B-form DNA and may have a stronger interaction with this motif, rendering longer bound time to mutant PAM. Furthermore, underwound DNA requires less energy to unwind the duplex, making it easier to form the R-loop. The combination of longer bound time to non-PAM and easier to unwind DNA duplex together leads to effective cleavage of non-PAM dsDNA in underwound topology.

bond. When C5 was mutated to T5, a steric clash could occur between the methyl group of thymine and the side chain of Asp1089. In support, mitigating the steric clash by either substituting aspartic acid with alanine or thymine with uracil strongly promoted cleavage activity to non-PAM targets. Together, these data unveil a new Cas9-PAM interaction mechanism, mediated by structure-guided docking into the DNA groove, and sequence-mediated interactions that include hydrogen bond and steric clash.

The topological properties of DNA, including DNA underwound (e.g., negative supercoiling, Z-DNA) and overwound (e.g., positive supercoiling), profoundly influence multiple aspects of the nucleic acid process (Baranello et al., 2012; Benham, 1979; Valdés et al., 2018; Valenti et al., 2011). Here, we found that DNA topology could affect the AtCas9-mediated genome-editing ability by interrogating PAM recognition step and DNA unwinding step. Underwound topology promotes the recognition of non-PAMs by strengthening the structure-dependent interaction of AtCas9 and target DNA. This is evident from AtCas9 producing cleavage in a crRNA-dependent manner at underwound non-PAM sites *in vitro* and in *E. coli*. Similarly, *in vitro* study of SpCas9 has shown that the mechanical distortion of DNA results in gRNA-dependent but PAM-independent off-target events at the single-molecule level (Newton et al., 2019), indicating that DNA topology may affect PAM recognition for other Cas proteins. DNA topology can also affect the DNA unwinding process as the torque residing within tangled strands is different among topoisomers (Sheinin et al., 2011). Previous studies have indicated that DNA supercoiling promotes DNA cleavage in WT PAM (Ivanov et al., 2020). Notably, our data using various topoisomers have indicated that a smaller torque residing in underwound DNA promotes cleavage, whereas a larger torque residing in overwound DNA requires higher energy to unwind the duplex. Collectively, DNA topology not only regulates DNA unwinding but also regulates PAM-Cas9 interaction. Our results unearthed a previously unknown factor that DNA topology regulates the PAM-Cas9 interaction and enables near-PAMless cleavage.

Base editors are one of the most powerful tools to correct genetic mutations, but PAM restriction has become a rate-limiting step to select effective gRNAs (Jinek et al., 2012). In this study, we identified a thermostable endonuclease AtCas9, which has the most relaxed PAM of CNNN and RNNA (R = A, G) at its optimal temperature. When presented with negatively supercoiled substrates in mammalian cells, the average cytosine base-editing efficiency was 46% with WT PAMs. When targeting supercoiled plasmids in *E. coli*, AtCas9 is able to cleave 16 PAMs and non-PAMs. Furthermore, AtCas9 is able to mediate efficient cytosine base editing in four endogenous loci, with a ~3.7-fold increase compared with that of xCas9 and comparable activity with SpRY. Similar to BE3, AtCas9-ABE8e is active in four loci tested, with a wide editing window. To our knowledge, the targeting scope of AtCas9 is the broadest among naturally occurring Cas orthologs known to function efficiently in mammalian cells.

Limitations of the study

When applying AtCas9 in mammalian genome editing, AtCas9 showed effective cleavage activity in lentivirus-generated EGFP or p53 loci. However, when editing endogenous loci, the cleavage activity was low. The low efficiency of AtCas9 may result from the chromosomal structure interference (e.g., preventing RNPs from approaching the target site, or the RNPs are bound at the target site but the protein conformation is not fully activated to accomplish the full cleavage of two strands), its compromised nuclease activity at 37°C, or different repair mechanisms after cleavage.

(E) Combined C-to-T editing efficiency of 25 gRNAs tested.
(F and G) Editing window of AtCas9-BE3 and SpRY-BE3 in selected gRNAs (F) or combined (G).
(H and I) A-to-G base-editing efficiency of AtCas9-ABE8e at four different loci with indicated PAMs.
(J and K) Editing window of AtCas9-ABE8e in selected gRNAs (J) or combined (K). Data are shown as mean ± SD. n ≥ 2 for the entire figure.

Further studies to enhance its cleavage activity at endogenous sites can be explored in the future.

STAR★METHODS

Detailed methods are provided in the online version of this paper and include the following:

- KEY RESOURCES TABLE
- RESOURCE AVAILABILITY
  - Lead contact
  - Materials availability
  - Data and code availability
- EXPERIMENTAL MODEL AND SUBJECT DETAILS
- METHOD DETAILS
  - RNA *in vitro* transcription
  - Protein purification
  - *In vitro* cleavage assay
  - *In vivo* PAM screen
  - *In vitro* PAM screen
  - Preparation of positive supercoiled plasmid and Z-DNA
  - Electrophoretic mobility shift assay (EMSA)
  - Plasmids and oligonucleotides
  - *In vivo* cleavage in *E.coli*
  - AtCas9-RNA-DNA structure simulation
  - Cell culture, transfection, GFP detection, and data analysis
  - GUIDE-seq
- QUANTIFICATION AND STATISTICAL ANALYSIS

SUPPLEMENTAL INFORMATION

Supplemental information can be found online at https://doi.org/10.1016/j.molcel.2022.09.032.

ACKNOWLEDGMENTS

We thank Erik Sontheimer for his suggestions on the manuscript, Pu Yingying for sharing MG1655 strain, and Ruijin Ji for graphic design of the model. We also thank the core facility in MRI of Wuhan University for technical assistance. This research was supported by the Ministry of Agriculture and Rural Affairs of China, the National Key R&D Program of China (2019YFA0802801 and 2018YFA0801401), National Science Foundation (grant no. 31972936, 32071442, and 31871345), the Fundamental Research Funds for the Central Universities (to Y.Z. and H.Y.), the Applied Basic Frontier Program of Wuhan City, and the startup funding from Wuhan University (to Y.Z. and H.Y., 2020020601012216).

AUTHOR CONTRIBUTIONS

Y.Z. designed and oversaw the entire project. Y.-J.S. and M.D. performed most of the experimental work and analyzed the data. J.-M.D. initiated the project. L.B., F.-Q.W., A.-H.H., and X.-L.L. helped with the experimental work. Y.-Z.Z., J.-Y.D., and C.-X.Z. performed bioinformatics analysis. Y.Z. and Y.-J.S. wrote the manuscript. H.Y. provided conceptual advice.

DECLARATION OF INTERESTS

Y.Z. and Y.-J.S. have a filed patent application (PCT/CN2022/077097). H.Y. is a founding member for CorrectSequence Therapeutics.

Received: March 22, 2022
Revised: August 4, 2022
Accepted: September 27, 2022
Published: October 21, 2022

REFERENCES

Anders, C., Niewoehner, O., Duerst, A., and Jinek, M. (2014). Structural basis of PAM-dependent target DNA recognition by the Cas9 endonuclease. Nature *513*, 569–573. https://doi.org/10.1038/nature13579.

Anzalone, A.V., Randolph, P.B., Davis, J.R., Sousa, A.A., Koblan, L.W., Levy, J.M., Chen, P.J., Wilson, C., Newby, G.A., Raguram, A., and Liu, D.R. (2019). Search-and-replace genome editing without double-strand breaks or donor DNA. Nature *576*, 149–157. https://doi.org/10.1038/s41586-019-1711-4.

Baranello, L., Levens, D., Gupta, A., and Kouzine, F. (2012). The importance of being supercoiled: how DNA mechanics regulate dynamic processes. Biochim. Biophys. Acta *1819*, 632–638. https://doi.org/10.1016/j.bbagrm.2011.12.007.

Barrangou, R., Fremaux, C., Deveau, H., Richards, M., Boyaval, P., Moineau, S., Romero, D.A., and Horvath, P. (2007). CRISPR provides acquired resistance against viruses in prokaryotes. Science *315*, 1709–1712. https://doi.org/10.1126/science.1138140.

Benham, C.J. (1979). Torsional stress and local denaturation in supercoiled DNA. Proc. Natl. Acad. Sci. USA *76*, 3870–3874. https://doi.org/10.1073/pnas.76.8.3870.

Bettotti, P., Visone, V., Lunelli, L., Perugino, G., Ciaramella, M., and Valenti, A. (2018). Structure and properties of DNA molecules Over the full range of biologically relevant supercoiling states. Sci. Rep. *8*, 6163. https://doi.org/10.1038/s41598-018-24499-5.

Bolger, A.M., Lohse, M., and Usadel, B. (2014). Trimmomatic: a flexible trimmer for Illumina sequence data. Bioinformatics *30*, 2114–2120. https://doi.org/10.1093/bioinformatics/btu170.

Bustamante, C., Bryant, Z., and Smith, S.B. (2003). Ten years of tension: single-molecule DNA mechanics. Nature *421*, 423–427. https://doi.org/10.1038/nature01405.

Chatterjee, P., Jakimo, N., and Jacobson, J.M. (2018). Minimal PAM specificity of a highly similar SpCas9 ortholog. Sci. Adv. *4*, eaau0766. https://doi.org/10.1126/sciadv.aau0766.

Chatterjee, P., Lee, J., Nip, L., Koseki, S.R.T., Tysinger, E., Sontheimer, E.J., Jacobson, J.M., and Jakimo, N. (2020). A Cas9 with PAM recognition for adenine dinucleotides. Nat. Commun. *11*, 2474. https://doi.org/10.1038/s41467-020-16117-8.

Chen, S., Zhou, Y., Chen, Y., and Gu, J. (2018). fastp: an ultra-fast all-in-one FASTQ preprocessor. Bioinformatics *34*, i884–i890. https://doi.org/10.1093/bioinformatics/bty560.

Chong, S., Chen, C., Ge, H., and Xie, X.S. (2014). Mechanism of transcriptional bursting in bacteria. Cell *158*, 314–326. https://doi.org/10.1016/j.cell.2014.05.038.

Clement, K., Rees, H., Canver, M.C., Gehrke, J.M., Farouni, R., Hsu, J.Y., Cole, M.A., Liu, D.R., Joung, J.K., Bauer, D.E., and Pinello, L. (2019). CRISPResso2 provides accurate and rapid genome editing sequence analysis. Nat. Biotechnol. *37*, 224–226. https://doi.org/10.1038/s41587-019-0032-3.

Collias, D., and Beisel, C.L. (2021). CRISPR technologies and the search for the PAM-free nuclease. Nat. Commun. *12*, 555. https://doi.org/10.1038/s41467-020-20633-y.

Couvin, D., Bernheim, A., Toffano-Nioche, C., Touchon, M., Michalik, J., Néron, B., Rocha, E.P.C., Vergnaud, G., Gautheret, D., and Pourcel, C. (2018). CRISPRCasFinder, an update of CRISRFinder, includes a portable version, enhanced performance and integrates search for Cas proteins. Nucleic Acids Res. *46*, W246–W251. https://doi.org/10.1093/nar/gky425.

Crooks, G.E., Hon, G., Chandonia, J.M., and Brenner, S.E. (2004). WebLogo: a sequence logo generator. Genome Res. *14*, 1188–1190. https://doi.org/10.1101/gr.849004.

Datsenko, K.A., Pougach, K., Tikhonov, A., Wanner, B.L., Severinov, K., and Semenova, E. (2012). Molecular memory of prior infections activates the CRISPR/Cas adaptive bacterial immunity system. Nat. Commun. *3*, 945. https://doi.org/10.1038/ncomms1937.

de la Fuente-Núñez, C., and Lu, T.K. (2017). CRISPR-Cas9 technology: applications in genome engineering, development of sequence-specific antimicrobials, and future prospects. Integr. Biol. (Camb) *9*, 109–122. https://doi.org/10.1039/c6ib00140h.

Doudna, J.A., and Charpentier, E. (2014). Genome editing. The new frontier of genome engineering with CRISPR-Cas9. Science *346*, 1258096. https://doi.org/10.1126/science.1258096.

Gao, L., Cox, D.B.T., Yan, W.X., Manteiga, J.C., Schneider, M.W., Yamano, T., Nishimasu, H., Nureki, O., Crosetto, N., and Zhang, F. (2017). Engineered Cpf1 variants with altered PAM specificities. Nat. Biotechnol. *35*, 789–792. https://doi.org/10.1038/nbt.3900.

Garneau, J.E., Dupuis, M.È., Villion, M., Romero, D.A., Barrangou, R., Boyaval, P., Fremaux, C., Horvath, P., Magadán, A.H., and Moineau, S. (2010). The CRISPR/Cas bacterial immune system cleaves bacteriophage and plasmid DNA. Nature *468*, 67–71. https://doi.org/10.1038/nature09523.

Gasiunas, G., Young, J.K., Karvelis, T., Kazlauskas, D., Urbaitis, T., Jasnauskaite, M., Grusyte, M.M., Paulraj, S., Wang, P.H., Hou, Z., et al. (2020). A catalogue of biochemically diverse CRISPR-Cas9 orthologs. Nat. Commun. *11*, 5512. https://doi.org/10.1038/s41467-020-19344-1.

Gaudelli, N.M., Komor, A.C., Rees, H.A., Packer, M.S., Badran, A.H., Bryson, D.I., and Liu, D.R. (2017). Programmable base editing of A•T to G•C in genomic DNA without DNA cleavage. Nature *551*, 464–471. https://doi.org/10.1038/nature24644.

Gong, S., Yu, H.H., Johnson, K.A., and Taylor, D.W. (2018). DNA unwinding is the primary determinant of CRISPR-Cas9 activity. Cell Rep. *22*, 359–371. https://doi.org/10.1016/j.celrep.2017.12.041.

Harrington, L.B., Burstein, D., Chen, J.S., Paez-Espino, D., Ma, E., Witte, I.P., Cofsky, J.C., Kyrpides, N.C., Banfield, J.F., and Doudna, J.A. (2018). Programmed DNA destruction by miniature CRISPR-Cas14 enzymes. Science *362*, 839–842. https://doi.org/10.1126/science.aav4294.

Herbert, A. (2019). Z-DNA and Z-RNA in human disease. Commun. Biol. *2*, 7. https://doi.org/10.1038/s42003-018-0237-x.

Hu, J.H., Miller, S.M., Geurts, M.H., Tang, W., Chen, L., Sun, N., Zeina, C.M., Gao, X., Rees, H.A., Lin, Z., and Liu, D.R. (2018). Evolved Cas9 variants with broad PAM compatibility and high DNA specificity. Nature *556*, 57–63. https://doi.org/10.1038/nature26155.

Ivanov, I.E., Wright, A.V., Cofsky, J.C., Aris, K.D.P., Doudna, J.A., and Bryant, Z. (2020). Cas9 interrogates DNA in discrete steps modulated by mismatches and supercoiling. Proc. Natl. Acad. Sci. USA *117*, 5853–5860. https://doi.org/10.1073/pnas.1913445117.

Jiang, F., and Doudna, J.A. (2017). CRISPR-Cas9 structures and mechanisms. Annu. Rev. Biophys. *46*, 505–529. https://doi.org/10.1146/annurev-biophys-062215-010822.

Jiang, F., Taylor, D.W., Chen, J.S., Kornfeld, J.E., Zhou, K., Thompson, A.J., Nogales, E., and Doudna, J.A. (2016). Structures of a CRISPR-Cas9 R-loop complex primed for DNA cleavage. Science *351*, 867–871. https://doi.org/10.1126/science.aad8282.

Jiang, W., Bikard, D., Cox, D., Zhang, F., and Marraffini, L.A. (2013). RNA-guided editing of bacterial genomes using CRISPR-Cas systems. Nat. Biotechnol. *31*, 233–239. https://doi.org/10.1038/nbt.2508.

Jinek, M., Chylinski, K., Fonfara, I., Hauer, M., Doudna, J.A., and Charpentier, E. (2012). A programmable dual-RNA-guided DNA endonuclease in adaptive bacterial immunity. Science *337*, 816–821. https://doi.org/10.1126/science.1225829.

Karvelis, T., Gasiunas, G., Young, J., Bigelyte, G., Silanskas, A., Cigan, M., and Siksnys, V. (2015). Rapid characterization of CRISPR-Cas9 protospacer adjacent motif sequence elements. Genome Biol. *16*, 253. https://doi.org/10.1186/s13059-015-0818-7.

Kim, M.G., Lee, J.C., Park, D.J., Li, W.J., and Kim, C.J. (2014). Alicyclobacillus tengchongensis sp. nov., a thermo-acidophilic bacterium isolated from hot spring soil. J. Microbiol. *52*, 884–889. https://doi.org/10.1007/s12275-014-3625-z.

Komor, A.C., Kim, Y.B., Packer, M.S., Zuris, J.A., and Liu, D.R. (2016). Programmable editing of a target base in genomic DNA without double-stranded DNA cleavage. Nature *533*, 420–424. https://doi.org/10.1038/nature17946.

Künne, T., Westra, E.R., and Brouns, S.J. (2015). Electrophoretic mobility shift assay of DNA and CRISPR-cas ribonucleoprotein complexes. Methods Mol. Biol. *1311*, 171–184. https://doi.org/10.1007/978-1-4939-2687-9_11.

Kuzminov, A. (2018). When DNA topology turns deadly - RNA polymerases dig in their R-loops to stand their ground: new positive and negative (super)twists in the replication-transcription conflict. Trends Genet. *34*, 111–120. https://doi.org/10.1016/j.tig.2017.10.007.

Leenay, R.T., Maksimchuk, K.R., Slotkowski, R.A., Agrawal, R.N., Gomaa, A.A., Briner, A.E., Barrangou, R., and Beisel, C.L. (2016). Identifying and visualizing functional PAM diversity across CRISPR-cas systems. Mol. Cell *62*, 137–147. https://doi.org/10.1016/j.molcel.2016.02.031.

Ma, E., Harrington, L.B., O'Connell, M.R., Zhou, K., and Doudna, J.A. (2015). Single-stranded DNA cleavage by divergent CRISPR-Cas9 enzymes. Mol. Cell *60*, 398–407. https://doi.org/10.1016/j.molcel.2015.10.030.

Makarova, K.S., Aravind, L., Wolf, Y.I., and Koonin, E.V. (2011a). Unification of Cas protein families and a simple scenario for the origin and evolution of CRISPR-Cas systems. Biol. Direct *6*, 38. https://doi.org/10.1186/1745-6150-6-38.

Makarova, K.S., Haft, D.H., Barrangou, R., Brouns, S.J., Charpentier, E., Horvath, P., Moineau, S., Mojica, F.J., Wolf, Y.I., Yakunin, A.F., et al. (2011b). Evolution and classification of the CRISPR-Cas systems. Nat. Rev. Microbiol. *9*, 467–477. https://doi.org/10.1038/nrmicro2577.

Marraffini, L.A., and Sontheimer, E.J. (2008). CRISPR interference limits horizontal gene transfer in staphylococci by targeting DNA. Science *322*, 1843–1845. https://doi.org/10.1126/science.1165771.

Marraffini, L.A., and Sontheimer, E.J. (2010). Self versus non-self discrimination during CRISPR RNA-directed immunity. Nature *463*, 568–571. https://doi.org/10.1038/nature08703.

Mekler, V., Minakhin, L., and Severinov, K. (2017). Mechanism of duplex DNA destabilization by RNA-guided Cas9 nuclease during target interrogation. Proc. Natl. Acad. Sci. USA *114*, 5443–5448. https://doi.org/10.1073/pnas.1619926114.

Newton, M.D., Taylor, B.J., Driessen, R.P.C., Roos, L., Cvetesic, N., Allyjaun, S., Lenhard, B., Cuomo, M.E., and Rueda, D.S. (2019). DNA stretching induces Cas9 off-target activity. Nat. Struct. Mol. Biol. *26*, 185–192. https://doi.org/10.1038/s41594-019-0188-z.

Nishimasu, H., Shi, X., Ishiguro, S., Gao, L., Hirano, S., Okazaki, S., Noda, T., Abudayyeh, O.O., Gootenberg, J.S., Mori, H., et al. (2018). Engineered CRISPR-Cas9 nuclease with expanded targeting space. Science *361*, 1259–1262. https://doi.org/10.1126/science.aas9129.

Oberstrass, F.C., Fernandes, L.E., and Bryant, Z. (2012). Torque measurements reveal sequence-specific cooperative transitions in supercoiled DNA. Proc. Natl. Acad. Sci. USA *109*, 6106–6111. https://doi.org/10.1073/pnas.1113532109.

Ondov, B.D., Bergman, N.H., and Phillippy, A.M. (2011). Interactive metagenomic visualization in a Web browser. BMC Bioinformatics *12*, 385. https://doi.org/10.1186/1471-2105-12-385.

Pickar-Oliver, A., and Gersbach, C.A. (2019). The next generation of CRISPR-Cas technologies and applications. Nat. Rev. Mol. Cell Biol. *20*, 490–507. https://doi.org/10.1038/s41580-019-0131-5.

Ran, F.A., Cong, L., Yan, W.X., Scott, D.A., Gootenberg, J.S., Kriz, A.J., Zetsche, B., Shalem, O., Wu, X., Makarova, K.S., et al. (2015). In vivo genome editing using Staphylococcus aureus Cas9. Nature *520*, 186–191. https://doi.org/10.1038/nature14299.

Rich, A., and Zhang, S. (2003). Timeline: Z-DNA: the long road to biological function. Nat. Rev. Genet. *4*, 566–572. https://doi.org/10.1038/nrg1115.

Richter, M.F., Zhao, K.T., Eton, E., Lapinaite, A., Newby, G.A., Thuronyi, B.W., Wilson, C., Koblan, L.W., Zeng, J., Bauer, D.E., et al. (2020). Phage-assisted evolution of an adenine base editor with improved Cas domain compatibility and activity. Nat. Biotechnol. *38*, 883–891. https://doi.org/10.1038/s41587-020-0453-z.

Rio, D.C. (2013). Expression and purification of active recombinant T7 RNA polymerase from E. coli. Cold Spring Harbor Protoc. *2013*. pdb.prot078527. https://doi.org/10.1101/pdb.prot078527.

Rousseau, B.A., Hou, Z., Gramelspacher, M.J., and Zhang, Y. (2018). Programmable RNA cleavage and recognition by a natural CRISPR-Cas9 system from Neisseria meningitidis. Mol. Cell *69*, 906–914.e4. https://doi.org/10.1016/j.molcel.2018.01.025.

Sheinin, M.Y., Forth, S., Marko, J.F., and Wang, M.D. (2011). Underwound DNA under tension: structure, elasticity, and sequence-dependent behaviors. Phys. Rev. Lett. *107*, 108102. https://doi.org/10.1103/PhysRevLett.107.108102.

Singh, D., Sternberg, S.H., Fei, J., Doudna, J.A., and Ha, T. (2016). Real-time observation of DNA recognition and rejection by the RNA-guided endonuclease Cas9. Nat. Commun. *7*, 12778. https://doi.org/10.1038/ncomms12778.

Sontheimer, E.J., and Barrangou, R. (2015). The bacterial origins of the CRISPR genome-editing revolution. Hum. Gene Ther. *26*, 413–424. https://doi.org/10.1089/hum.2015.091.

Sternberg, S.H., LaFrance, B., Kaplan, M., and Doudna, J.A. (2015). Conformational control of DNA target cleavage by CRISPR-Cas9. Nature *527*, 110–113. https://doi.org/10.1038/nature15544.

Sternberg, S.H., Redding, S., Jinek, M., Greene, E.C., and Doudna, J.A. (2014). DNA interrogation by the CRISPR RNA-guided endonuclease Cas9. Nature *507*, 62–67. https://doi.org/10.1038/nature13011.

Stolz, R., Sulthana, S., Hartono, S.R., Malig, M., Benham, C.J., and Chedin, F. (2019). Interplay between DNA sequence and negative superhelicity drives R-loop structures. Proc. Natl. Acad. Sci. USA *116*, 6260–6269. https://doi.org/10.1073/pnas.1819476116.

Szczelkun, M.D., Tikhomirova, M.S., Sinkunas, T., Gasiunas, G., Karvelis, T., Pschera, P., Siksnys, V., and Seidel, R. (2014). Direct observation of R-loop formation by single RNA-guided Cas9 and Cascade effector complexes. Proc. Natl. Acad. Sci. USA *111*, 9798–9803. https://doi.org/10.1073/pnas.1402597111.

Terns, R.M., and Terns, M.P. (2014). CRISPR-based technologies: prokaryotic defense weapons repurposed. Trends Genet. *30*, 111–118. https://doi.org/10.1016/j.tig.2014.01.003.

Tsai, S.Q., Zheng, Z., Nguyen, N.T., Liebers, M., Topkar, V.V., Thapar, V., Wyvekens, N., Khayter, C., Iafrate, A.J., Le, L.P., et al. (2015). GUIDE-seq enables genome-wide profiling of off-target cleavage by CRISPR-Cas nucleases. Nat. Biotechnol. *33*, 187–197. https://doi.org/10.1038/nbt.3117.

Valdés, A., Segura, J., Dyson, S., Martínez-García, B., and Roca, J. (2018). DNA knots occur in intracellular chromatin. Nucleic Acids Res. *46*, 650–660. https://doi.org/10.1093/nar/gkx1137.

Valenti, A., Perugino, G., Rossi, M., and Ciaramella, M. (2011). Positive supercoiling in thermophiles and mesophiles: of the good and evil. Biochem. Soc. Trans. *39*, 58–63. https://doi.org/10.1042/BST0390058.

Wagih, O. (2017). ggseqlogo: a versatile R package for drawing sequence logos. Bioinformatics Oxf. Engl. *33*, 3645–3647. https://doi.org/10.1093/bioinformatics/btx469.

Walton, R.T., Christie, K.A., Whittaker, M.N., and Kleinstiver, B.P. (2020). Unconstrained genome targeting with near-PAMless engineered CRISPR-Cas9 variants. Science *368*, 290–296. https://doi.org/10.1126/science.aba8853.

Wiedenheft, B., Sternberg, S.H., and Doudna, J.A. (2012). RNA-guided genetic silencing systems in bacteria and archaea. Nature *482*, 331–338. https://doi.org/10.1038/nature10886.

Yosef, I., Goren, M.G., and Qimron, U. (2012). Proteins and DNA elements essential for the CRISPR adaptation process in Escherichia coli. Nucleic Acids Res. *40*, 5569–5576. https://doi.org/10.1093/nar/gks216.

Zhang, Y., Cui, Y., An, R., Liang, X., Li, Q., Wang, H., Wang, H., Fan, Y., Dong, P., Li, J., et al. (2019). Topologically constrained formation of stable Z-DNA from normal sequence under physiological conditions. J. Am. Chem. Soc. *141*, 7758–7764. https://doi.org/10.1021/jacs.8b13855.

Zhang, Y., Rajan, R., Seifert, H.S., Mondragón, A., and Sontheimer, E.J. (2015). DNase H activity of Neisseria meningitidis Cas9. Mol. Cell *60*, 242–255. https://doi.org/10.1016/j.molcel.2015.09.020.

Please cite this article in press as: Shi et al., DNA topology regulates PAM-Cas9 interaction and DNA unwinding to enable near-PAMless cleavage by thermophilic Cas9, Molecular Cell (2022), https://doi.org/10.1016/j.molcel.2022.09.032

STAR★METHODS

KEY RESOURCES TABLE

REAGENT or RESOURCE	SOURCE	IDENTIFIER
Bacterial and virus strains		
E. coli strain DH5-alpha	Weidi Biotechnology	**DL1001**
E. coli strain BL21	Weidi Biotechnology	EC1002
E. coli strain MG1655	Yingying Pu Lab	N/A
Chemicals, peptides, and recombinant proteins		
T4 DNA Ligase	New England Biolabs	M0202
T4 PolyNucleotide Kinase (PNK)	New England Biolabs	M0201
Bbs I-HF	New England Biolabs	R3539
Bsa I-HFv2	New England Biolabs	R3733
Nt.BspQ I	New England Biolabs	R0644
RSR II	New England Biolabs	R0501
Pci I	New England Biolabs	R0655
EcoR I-HF	New England Biolabs	R3101
Exonuclease I	New England Biolabs	M0293
CircLigase™ ssDNA Ligase	Lucigen	CL4111K
S1 nuclease	Thermo Fisher	EN0321
Proteinase K	Thermo Fisher	EO0491
Phanta polymerase	Vazyme	d505-03
chloroquine	Sigma	C6628
Hoechst 33342	Thermo Fisher	H3570
Critical commercial assays		
Zymo DNA Clean & Concentrator kit	Zymo	D4034
Monarch® RNA Cleanup Kit (50 μg)	New England Biolabs	T2040
plasmid mini extract kit	OMEGA	D6943-02
HiPure total DNA mini kit	MAGEN	D3121-03
Hipure PCR Pure Mini Kit	MAGEN	D2121-03
5min™ TA/Blunt-Zero Cloning Kit	Vazyme	C601-02
E.Z.N.A. Gel Extraction Kit	OMEGA	D2500-02
VAHTS Universal DNA Library Prep Kit for Illumina V3	Vazyme	ND607-01
Label IT® Tracker™ Intracellular Nucleic Acid Localization Kit	Mirus Bio	MIR 7021
ClonExpress II One Step Cloning Kit	Vazyme	C112-02
Deposited data		
All raw FASTQ files for Miseq	This study	NCBI: SAMN30626197
unprocessed agarose or PAGE gels and microscopy data	This study	Mendeley Data: https://doi.org/10.17632/krdtc69m3x.1
Experimental models: Cell lines		
HEK293T	ATCC	CRL-3216
Oligonucleotides		
50nt 21aPAM3-TS CY5	GenScript	N/A
50nt 21aPAM-TS CY3	GenScript	N/A
120nt 21aPAM3-TS FAM	GenScript	N/A
120nt 21aPAM3-NTS 0 bulge	GenScript	N/A

(*Continued on next page*)

Continued

REAGENT or RESOURCE	SOURCE	IDENTIFIER
120nt 21aPAM3-NTS 1-2 bulge	GenScript	N/A
120nt 21aPAM3-NTS 3-4 bulge	GenScript	N/A
120nt 21aPAM3-NTS 5-6 bulge	GenScript	N/A
120nt 21aPAM3-NTS 19-20 bulge	GenScript	N/A
120nt 21aPAM3-NTS 21-22 bulge	GenScript	N/A
120nt 21aPAM3-NTS 23-25 bulge	GenScript	N/A
120nt 21aPAM3-NTS ctrl bulge	GenScript	N/A
50nt 21aPAM3-5U-NTS	GenScript	N/A
50nt 21aPAM-5mC-NTS	GenScript	N/A
Spacer and designed sgRNA sequences	This paper; See Table S1	N/A
Primers for PCR and high-throughput sequencing	Sangon Biotech; See Table S1	N/A
Recombinant DNA		
PAM library plasmid contains 21a spacer	This paper	N/A
pCE2-21a-PAM plasmids	This paper	N/A
pAT301 (expressing wild-type AtCas9 for cleavage in mammalian cells)	This paper	N/A
pRY301 (expressing wild-type SpRY for cleavage in mammalian cells)	This paper	N/A
pAT7.2 (expressing AtCas9-BE3 for CBE in mammalian cells)	This paper	N/A
pSpRY (expressing SpRY-BE3 for CBE in mammalian cells)	This paper	N/A
pAT8.5 (expressing AtCas9-ABE8e for ABE in mammalian cells)	This paper	N/A
Gcl200 (AtCas9 sgRNA expressing plasmid contains full length scaffold)	This paper	N/A
Gcl202 (AtCas9 sgRNA expressing plasmid contains truncated scaffold)	This paper	N/A
Gcl203 (AtCas9 sgRNA expressing plasmid contains truncated scaffold)	This paper	N/A
pACYC184-AtCas9 locus (expressing wild-type AtCas9 for cleavage in *E. coli*)	This paper	N/A
pCas-SpRY (expressing wild-type SpRY for cleavage in *E. coli*)	This paper	N/A
pET28a-His-AtCas9 (AtCas9 protein purification)	This paper	N/A
Software and algorithms		
Image Lab	Bio-rad	https://www.bio-rad.com/en-us/product/image-lab-software?ID=KRE6P5E8Z
FlowJo	FlowJo.LLC	https://www.flowjo.com/
Prism 6	GraphPad	https://www.graphpad.com/
CRISPResso2	Github	https://github.com/pinellolab/
Other		
penicillin-streptomycin	Hyclone	113-98-4
0.05% pancreatin	Gibco	25300-054

RESOURCE AVAILABILITY

Lead contact

Further information and requests for resources and reagents should be directed to and will be fulfilled by the lead contact, Ying Zhang (ying.zhang84@whu.edu.cn).

Materials availability

All unique reagents generated in this study are available from the lead contact with a completed Materials Transfer Agreement.

Data and code availability

- Raw FASTQ files are deposited in the SRA and the accession number is provided in the key resources table. Unprocessed agarose or PAGE gels and microscopy data have been deposited at Mendeley Data and are publicly available as of the date of publication, and the DOI is provided in the key resources table.
- This paper does not report original code.
- Any additional information required to reanalyze the data reported in this paper is available from the lead contact upon request.

EXPERIMENTAL MODEL AND SUBJECT DETAILS

DH5-alpha or MG1655 electrocompetent *E. coli* cells (Weidi Biotechnology) were transformed with the PAM library plasmids (GenScript) or target plasmids. Cells of BL21 (DE3) strain of *E. coli* (Weidi Biotechnology) were transformed with protein expression plasmids. Human HEK 293T cells and its derivative reporter cell line (HEK293T-EGFP and HEK293T-p53-(+1frame shifted)-EGFP cell line) were maintained in DMEM (Thermo Fisher Scientific) with 10% fetal bovine serum (FBS) (AusGenex) and 1% Penicillin/Streptomycin (Corning) in a 37°C incubator with 5% CO_2.

METHOD DETAILS

RNA *in vitro* transcription

RNA was *in vitro* transcribed using synthetic DNA oligos carrying a T7 promoter sequence. After transcription with T7 RNA polymerase at 37°C for 1 hour, tracrRNA, crRNA or sgRNA were purified using column or gel purification kit (NEB or ZYMO) according to the manufactory protocols. Primers and oligonucleotides used in this study were listed in Table S1.

Protein purification

6xHis tagged AtCas9 gene was synthesized and cloned into pET28a vector (GenScript). The recombinant plasmid was transformed into *E.coli* BL21 (DE3) and protein expression was induced by adding 0.5mM IPTG. After incubating at 18°C for 16h, cell pellets were resuspended in lysis buffer (20mM Tris-HCl, 500mM NaCl, 10% glycerol, pH7.4) and lysed by sonication (Scientz). Supernatant was collected after centrifugation and then filtered with 0.22 micron filters. Affinity purification followed by size exclusion chromatographic step were performed for protein purification. In brief, clarified lysate was loaded to HisTrap HP (GE Healthcare) in NGC Quest 10 Chromatography System (Biorad). Column is pre-balanced in lysis buffer. Protein were eluted in buffer B1 (20mM Tris-HCl, 500mM NaCl, 500mM Imidazole, 10% glycerol, pH7.4) using gradient program. Different elution fractions were collected and then verified by SDS-PAGE to identify target protein. Affinity purified protein was then loaded to Superdex 200 Increase 10/300 GL column (GE Healthcare) in buffer B2 (20mM Tris-HCl, 200mM NaCl, 20% glycerol, pH7.4). Eluted protein was concentrated by centrifugal filters (Millipore) and stored in buffer B2 at -80°C. AtCas9 D8A, H617A/N640A, D8A/H617A/N640A and PI-V4∼13 mutants were generated using the site-directed mutation PCR and confirmed by DNA sequencing. AhCas9 gene were synthesized and cloned into the same expression vector (GenScript). The proteins were purified following the same procedure as for the wild-type AtCas9 protein.

T7 RNA polymerase, SpCas9, NmeCas9 and Cas14a1 were purified according to the previous study (de la Fuente-Núñez and Lu, 2017; Harrington and Burstein, 2018; Rio, 2013; Rousseau et al., 2018). In short, T7 RNA polymerase gene and SpCas9/NmeCas9/Cas14a1 genes were synthesized (GenScript) and cloned into pET30c or pET28a vector respectively. T7 RNA polymerase expression was induced with 1mM IPTG at 37°C for 4h, and SpCas9, NmeCas9, or Cas14a1 was induced with 0.5mM IPTG at 25°C for 10h. Reverse gyrase gene were synthesized and cloned into pET28a vector (GenScript), and the protein was induced at 20°C for 14h under 0.1mM IPTG. The protein purification steps were the same as AtCas9.

In vitro cleavage assay

Unless noted elsewhere, purified AtCas9 protein (50nM) and crRNA:tracrRNA duplex (50nM, 1:1) were mixed in buffer16 (10mM KCl, 20mM HEPES, 10mM $MgCl_2$, 0.5mM DTT, 0.1mM EDTA, pH7.9), and incubated at room temperature for 10 minutes. DNA substrate was added to the reaction system in the final concentration of 3nM (plasmid DNA or linear dsDNA longer than 2kb) and incubated at 55°C for 30min. Cleavage of fluorescently labeled oligonucleotides were performed with 100nM AtCas9 RNP incubated with 10nM substrates in buffer 16 at 55°C for 30min. The reactions were stopped by adding 1μl Proteinase K (Thermo Fisher) at 55°C for 10min. Cleaved products were resolved by 0.8% TAE agarose gel and visualized by ethidium bromide staining for plasmid DNA, 12% native PAGE or denature PAGE for fluorescently labeled oligonucleotides. Cleavage of Z-form DNA in Figure 2D was performed by incubating 200nM AtCas9 RNP with 55nM substrates for 50min at 55°C. Quantification were performed using Image Lab software (Bio-rad) and cleavage efficiency were plotted using Prism 6 (GraphPad).

Please cite this article in press as: Shi et al., DNA topology regulates PAM-Cas9 interaction and DNA unwinding to enable near-PAMless cleavage by thermophilic Cas9, Molecular Cell (2022), https://doi.org/10.1016/j.molcel.2022.09.032

In vivo PAM screen

The PAM plasmid library containing the protospacer 21a and 8 nucleotides randomized PAM sequences were synthesized and cloned into pUC19 vector (GenScript). The pooled plasmid library (100ng) were transformed into electrocompetent *E.coli* harbouring a AtCas9 locus (pACYC184-AtCas9), SpCas9 locus (pCas9-21) or a control plasmid with no locus (pACYC184). After transformation, cells were grown in selective medium containing ampicillin (50μg/ml) and chloramphenicol (25μg/ml) for 16h at 37°C. Plasmid DNA was extracted and purified using plasmid mini kit (Omega). The target PAM region was amplified with primers containing adapters for Illumina NovaSeq. NovaSeq reads were filtered by an average Phred quality (Q score) >25. The 8 nucleotides randomized PAM was extracted and analyzed with Python script. Normalization was performed against control sample in which Cas9 was not expressed to calculate sequencing or PCR bias. The figures were draw by R (Wagih, 2017).

In vitro PAM screen

The PAM plasmid library described previously were treated with BsaIor Nt.BspQI(NEB) to generate linear or open circle topology respectively. Column purified linear, open circle or negative supercoiled PAM library DNA (10nM) were then digested with AtCas9-crRNA-tracrRNA complex at 100nM concentration and incubated at 55°C for 30 min. More stringent cleavage assays were performed with reduced RNP to substrate ration at indicated doses and temperature. Cleaved products were resolved on 0.8% TAE agarose gel and cleaved bands were gel extracted. The target PAM region was amplified with adapters (Vazyme) for NovaSeq. NovaSeq reads were required to be filtered by an average Phred quality (Q score) at least 25. The 8 nucleotides randomized PAM was extracted and analyzed with Python script. Raw reads were normalized according to the control which is digested by restriction enzyme EcoR I. The seqlogo figures were draw by R (Wagih, 2017). In order to correspond to seglogo plot, the 8N randomized PAM was separated into two 4N PAM according to position. PAM wheel was draw by plotting individual nucleotides accordingly (Leenay et al., 2016; Ondov et al., 2011).

Preparation of positive supercoiled plasmid and Z-DNA

Positive supercoiling

5nM negative supercoiled plasmid pCE2-PAM1 or pCE2-PAM3 was incubated with various concentrations of Reverse Gyrase (5nM, 50nM, 250nM) in RG buffer (35mM Tris-HCl, 0.1mM Na_2EDTA, 30mM $MgCl_2$, 2mM DTT, 1mM ATP) in a final volume of 20μl (Bettotti et al., 2018). After incubating at 80°C for 10 minutes, the samples were purified and analyzed on 1% TAE agarose gel with 0μM or 20μM chloroquine (Sigma). Gels were stained with ethidium bromide.

Z-DNA

The preparation of Z-DNA was modified from previous study (Zhang et al., 2019). Two single-stranded DNA circles were prepared separately and then hybridized to form a Z-form and B-form DNA hybrid (Zhang et al., 2019). In brief, 89nt single-stranded DNA with 5'-phosphate and 3'-hydroxyl groups were synthesized and circularized using CirLigase (Lucigen) to form DNA circle. The circularization reaction was carried out at 60°C for 2h, and then followed by ExonucleaseI(NEB) to remove the linear DNA at 37°C for 2h. The cyclization products were recovered and the single-stranded DNA circle (cF-89) and its complementary circle (cR-89) were annealed in annealing buffer (10mM HEPES, 10mM $MgCl_2$, pH7.5) to generate a B-form and Z-form hybrid double-stranded DNA circle (CC). Samples were analyzed on 8% native PAGE, and hybrid double-stranded DNA circles were column purified using Zymo DNA Clean & Concentrator kit (Zymo). Validation of Z-DNA were performed by treating with S1 nuclease (Thermo Fisher), which recognized Z-B junction and resulted a double-stranded break at the recognition site (Zhang et al., 2019). 0.2μM Z-B chimera hybrid was treated with S1 nuclease (2U) in 20μl reaction buffer. After incubating at room temperature for 1h, the reaction was terminated by adding 2μl EDTA (0.5M, pH8.0) and heat-inactivated at 70°C for 10min. The linear products were resolved by 12% native PAGE.

Electrophoretic mobility shift assay (EMSA)

dAtCas9 and sgRNA were mixed at 1:2 molar ratio in buffer16 (10mM KCl, 20mM HEPES, 10mM $MgCl_2$, 0.5mM DTT, 0.1mM EDTA, pH7.9). After incubation at room temperature for 10 minutes, the RNP mixture were diluted to various concentration ranging from 2.4μM to 1.2nM, and 4nM cy5-labeled oligonucleotides was added. Binding reactions were carried out at 55°C for 30 minutes. Samples were resolved on 4% native TBE-PAGE for oligonucleotides. The EMSA binding assay for dSpCas9 was performed under the same buffer and incubated at 37°C for 30 minutes. For plasmid substrate binding assay, we first generated 1551bp mini plasmid from pCE2-PAM1 or pCE2-PAM3 vector by digesting with RSRII and PciI enzymes. Mini plasmids were sequence verified and labeled with Cy5 kit according to the manufactory protocol (Mirus Bio). 1nM cy5-labeled negative supercoil plasmid or NcoI-linearized plasmid containing WT PAM (CTAA) or mutated PAM (TGAC) were incubated with dAtCas9 RNP complex at indicated dosage. Binding reactions were resolved on 0.8% agarose gel in sodium boric acid (SB) buffer (8.6mM sodium borate, 45mM boric acid, pH8.3) for 11h at 20mA at 4°C (Künne et al., 2015). Gels were imaged by Biorad Chemidoc MP imager (Bio-rad).

Plasmids and oligonucleotides

In order to construct plasmids containing 16 different PAM combinations for cleavage, oligonucleotides carrying 21a protospacer and 16 PAM sequences were synthesized from Sango Biotech. Oligos were annealed in annealing buffer (10mM Tris-HCl, 20mM NaCl, pH8.0) at 95°C for 5 minutes and then ramp down to 25°C at 0.1°C/s. Annealed duplexed oligonucleotides were ligated to the pCE2 vector by using TA/Blunt-Zero Cloning Kit (Vazyme). For editing negative supercoiled substrates in mammalian cells,

oligonucleotide carrying protospacer 36 and sixteen PAM sequences as well as their complementary strands were synthesized (Sangon Biotech), annealed and ligated to modified lentiCRISPR v2 vector (Addgene plasmid 52961), in which spCas9 and sgRNA scaffold was removed.

U6 promoter-driven AtCas9 sgRNA mammalian expression plasmid (named Gcl) was generated by replacing the sgRNA scaffold sequence in the gRNA_cloning Vector (Addgene plasmid 41824) with the AtCas9 sgRNA scaffold by Gibson assembly using ClonExpress II One Step Cloning Kit (Vazyme). SgRNA cloning were constructed by phosphorylation of oligonucleotides corresponding to spacer sequences with PNK (NEB), annealing and ligating into BbsI-digested Gcl vector.

The AtCas9 nuclease mammalian expression plasmid (named pAT301) was generated by cloning the codon optimized AtCas9 sequence (GenScript) into the EcoRI and AgeI sites of pX330 (Addgene plasmid 42230), replacing the promoter and nuclear localization signal with TT5 promoter and 2*cmyc-nucleoplasmin as well as removing U6 and sgRNA scaffold by Gibson assembly cloning (Vazyme). AtCas9-CBE expression plasmids (named pAT7.2) was generated by replacing the Cas9 sequence and nuclear localization signal in the pLenti-FNLS-P2A-Puro Vector (Addgene plasmid 110841) with AtCas9 (D8A) and 2*cmyc-nucleoplasmin by Gibson assembly cloning. xCas9-BE3 and SpRY-BE3 expression plasmids was generated by replacing Cas9 sequence from xCas9(3.7)-BE3 vector (Addgene plasmid 108380) into pAT7.2 by Gibson assembly. AtCas9-ABE8e expression plasmids (named pAT8.5) was generated by replacing the Cas9 sequence and the promoter in pAT301 with AtCas9 (D8A) and CMV promoter as well as adding an adenosine deaminase (TadA-8e) by Gibson assembly cloning.

In vivo cleavage in *E.coli*

For Figure 1B, *E.coli* cells harboring a AtCas9 expressing plasmid were transfected with targeted or mismatch protospacer PAM library plasmids and cell densities were measured every hour. For negative control, matched protospacer PAM library plasmids were transfected into control *E.coli*. For positive control, plasmids expressing AtCas9 locus and its matched protospacer with CNNA PAM were co-transfected into control *E.coli*.

For Figures 2I and S4D, AtCas9 or dAtCas9, SpRY CRISPR mini locus containing 21a spacer sequences and chloramphenicol expression fragment was amplified from pACYC184-AtCas9 or pCas9-21 using the primer pairs yz101-LHA-lacA-F and yz102-LacA-LHA-R, and this fragment was integrated into the LacA locus in *E.coli* MG1655 genome. The newly generated electrocompetent *E.coli* strain, MG1655-AtCas9 or MG1655-SpRY, was transformed with the plasmids harboring 21a protospacer followed by 16 PAM combinations for AtCas9 or 5 PAM combinations for SpRY. The transformed cells were plated on chloramphenicol (25μg/ml) or chloramphenicol (25μg/ml)/kanamycin (50μg/ml) LB plates to calculate total CFU or resistant CFU respectively. Transformation frequencies were determined as antibiotic resistant cfu/ml and total cfu/ml from six independent experiments.

AtCas9-RNA-DNA structure simulation

Structure simulation of AtCas9 was generated using AlphaFold2 and SWISS-MODEL and PyMOL software was used to assemble AtCas9-RNA-DNA complex.

Cell culture, transfection, GFP detection, and data analysis

Human HEK 293T cells and its derivative reporter cell line were maintained in DMEM with 10% FBS and 1% Penicillin/Streptomycin in a 37°C incubator with 5% CO_2. HEK293T-EGFP cell line was generated by stably incorporating a EF1α-EGFP vector into genome by lentivirus. HEK293T-p53-(+1frame shifted)-EGFP cell line was generated by stably incorporating a EF1α-p53-(+1frame shifted)-EGFP vector by lentivirus. Single copy integration colonies was selected by FACS sorting (BD FACSAria III) and cells were maintained on hygromycin supplemented selection medium.

For *in vivo* genome cleavage and cytosine base editor experiments, 1×10^5 cells were seeded into 24-well plates one day prior to transfection. 600ng of AtCas9, AtCas9-BE3, xCas9-BE3 or SpRY-BE3 expression plasmids and 400ng of sgRNA expression plasmids were co-transfected into HEK293T, HEK293T-EGFP cells or HEK293T-p53-(+1frame shifted)-EGFP cell line by calcium phosphate precipitation method. FACS analysis of GFP negative cells for *EGFP* locus or GFP positive cells for *p53* locus were performed 5 days post transfection using Novocyte (Agilent). When editing negative supercoiled substrates, 600ng pAT7.2 and 400ng gcl203 harboring spacer 36 were co-transfected with 1ng plasmids encoding PAM variants into HEK293T cells. Genomic DNA or plasmids was extracted four days post transfection using 50mM NaOH at 95°C for 10 minutes, and neutralized with 1M Tris-HCl (pH8.0). The editing locus were amplified and prepared for amplicon sequencing (Illumina).

For adenosine base editor experiments, 1.5ug of AtCas9-ABE and 750ng of sgRNA expression plasmids, pAT8.5 and gcl203, were mixed in 20ul electroporation buffer and transfected into 4×10^5 cells using Lonza 4D-Nucleofector following the manufacturer's protocol (Lonza). Genomic DNA was extracted three days post transfection and the editing locus were amplified and prepared for amplicon sequencing (Illumina).

Imaging of AtCas9 nuclear localization were performed by fixing transfected cells with 2% formaldehyde for 10 min at room temperature. Cells were counterstained with Hoechst (Life Technologies) and imaged under fluorescence microscopy (Nikon).

Amplicon sequencing of modified sites were performed to measure indel and base-editing efficiency. In brief, indel% was calculated by taking reads that contained indels and divided by total reads. Base editing efficiency was calculated by taking reads that contained the highest converted base changes and divided by total reads. The cutoff threshold was set at 0.02% as reads below 0.02% were largely sequencing noise. Indel profiles displayed in Figure S8 were drew by using CRISPResso2 (Clement et al., 2019) to align reads

to the reference sequence. Raw reads from High-throughput sequencing were merged using fastp software (Chen et al., 2018) to generate full-length reads. Trimmomatic tools (Bolger et al., 2014) was used to discard reads with a mean quality score <30 or adaptor contamination.

GUIDE-seq

GUIDE-seq experiments were performed by co-transfecting 1.5ug of pAT301, 750ng of gcl203 and 5pmol dsODN into 4×10^5 cells using Lonza 4D-Nucleofector following the manufacturer's protocol (Lonza). Genomic DNA was extracted three days post transfection and was sheared to an average length of 200bp by Covaris S200 instrument. Library was prepared through end repair and A-tail addition, followed by adapter ligation using VAHTS Universal DNA Library Prep Kit (Vazyme). Integration sites were amplified using oligo specific primers and sequenced using illumine platform. GUIDE-seq data was analyzed by guideseq v1.0.2 as previously described (https://github.com/aryeelab/guideseq). A PAM of VNNN and a maximum five mismatch was used to filter the data. To evaluate cleavage using plasmids bearing variable PAM, 1ng 1.5ug of pAT301, 750ng of gcl203 harboring spacer CMYC-6 and 5pmol dsODN were co-transfected with 1ng plasmids encoding PAM variants into 4×10^5 cells using Lonza 4D-Nucleofector. Genomic DNA was extracted three days post transfection, the genome and plasmid editing locus were amplified respectively and prepared for amplicon sequencing (Illumina).

QUANTIFICATION AND STATISTICAL ANALYSIS

Quantification of gel maps from *in vitro* cleavage and binding experiments was performed using Image Lab software (Bio-rad), and the efficiency were plotted using Prism 6 (GraphPad). Three independent experiments were performed and data were fitted with non-linear regression for kinetic analysis of cleavage efficiency and the equilibrium dissociation constant (Kd).

Residence time of AtCas9-RNP on negative supercoiled competitor DNA reported in Figure 4B was analysed following the cleavage competition assays protocol (Sternberg et al., 2014). In brief, the conditional survival probability of the florescence labeled target DNA, S*(t), is calculated using the formula below.

$$S^*(t) = \frac{s(t) - s(\infty)}{1 - s(\infty)}$$

The reaction rarely proceeds to completion, therefore $S(\infty)$ is defined as the survival probability of substrate DNA after 2 hour. For each reaction, we then obtained the change in the survival probability of the target DNA in the presence of competitor, $\Delta PS(t)$. Finally, the amount of time that RNP spent on the competitor DNA during the reaction was represented by integrate $\Delta PS(t)$ over the 2 hour reaction time. In the presence of competitor DNA, the decrease in cleavage rate is proportional to the time RNP spends bound to each competitor. In each reaction, the time RNP spends interrogating competitor cumulatively slows down the overall reaction.

For experiments in mammalian cells, values and error bars reflect mean ± s.d. of $n \geq 2$ or 3 independent biological replicates using Prism 6 (GraphPad).